Nano Materials Science xxx (xxxx) xxx

Contents lists available at ScienceDirect

Nano Materials Science

journal homepage: www.keaipublishing.com/cn/journals/nano-materials-science/

MXene-based electrochemical (bio) sensors for sustainable applications: Roadmap for future advanced materials

Qing Wang [a,1], Ning Han [b,1,*], Zhangfeng Shen [c], Xue Li [d], Zhijie Chen [e], Yue Cao [a,**], Weimeng Si [a], Fagang Wang [a,***], Bing-Jie Ni [e], Vijay Kumar Thakur [f,g,h,****]

[a] School of Material Science and Engineering, Shandong University of Technology, Zibo, 255000, China
[b] Department of Materials Engineering, KU Leuven, Leuven, 3001, Belgium
[c] College of Biological, Chemical Science and Engineering, Jiaxing University, Jiaxing, 314001, China
[d] School of Chemistry and Chemical Engineering, Shandong University of Technology, Zibo, 255000, China
[e] Centre for Technology in Water and Wastewater, School of Civil and Environmental Engineering, University of Technology Sydney, NSW, 2007, Australia
[f] Biorefining and Advanced Materials Research Center, SRUC, Edinburgh, EH9 3JG, United Kingdom
[g] School of Engineering, University of Petroleum & Energy Studies (UPES), Dehradun, 248007, Uttarakhand, India
[h] Centre for Research & Development, Chandigarh University, Mohali, 140413, Punjab, India

ARTICLE INFO

Keywords:
MXenes
Electrochemical sensors
Biomarkers
Pesticides

ABSTRACT

MXenes are emerging transition metal carbides and nitrides-based 2D conductive materials. They have found wide applications in sensors due to their excellent valuable properties. This paper reviews the recent research status of MXene-based electrochemical (bio) sensors for detecting biomarkers, pesticides, and other aspects. The first part of this paper introduced the synthesis strategy and the effect of surface modification on various properties of MXenes. The second part of this paper discussed the application of MXenes as electrode modifiers for detecting pesticides, environmental pollutants, and biomarkers such as glucose, hydrogen peroxide, etc. Hope this review will inspire more efforts toward research on MXene-based sensors to meet the growing requirements.

1. Introduction

In 2011, Prof. Gogotsi and coworkers reported a new 2D layer material.named MXenes that combine preeminent electrical conductivity with a hydrophilic surface [1]. The MXenes are 2D materials can be obtained by selective removal of the "A" layers from the layered carbides or carbonitrides. The MAX has a general formula of $M_{n+1}AX_n (n = 1, 2, 3)$, where M represents a transition metal; A represents a group IIIA and IVA element of the periodic table); and X is either C and/or N. [2]. Fig. 1 shows elements employed for the formation of MAX phases. The MXene was initially synthesized by etching of A element using a hydrofluoric acid (HF) solution [1]. As a result, the surface of MXenes is terminated with wealthy functional groups such as –F, –O and –OH, whose type depend on the etching route [3,4]. $Ti_3C_2T_x$ was the first MXene reported in 2011, followed by the synthesis of 19 different MXenes. There are dozens of predicted in computer simulation studies [5–7]. MXenes are a large family with a wide variety of species.

For mxenes, there are two commonly used synthetic routes, namely top-down and bottom-up synthesis methods.The former refers to etching of A element from the MAX phase with HF solution. At room temperature, the aluminum element in the MAX phase (Ti_3AlC_2) is selectively etched away with hydrofluoric acid, and the most widely used MXene, aluminum carbon titanium ($Ti_3C_2T_x$), is obtained [8–10]. Furthermore, as bottom-up methods, atomic layer deposition and chemical vapour deposition have also been used to synthesize Mxene [3]. In last several years, in addition to the reaction system of HF solution, other synthesis ways have also emerged, which are used for catalysts, seawater desalination, electrochemistry, wearable electronic devices, electromagnetic interference shielding, and electrode materials, providing much more applied potential [11–15]. Compared to other materials that people are

* Corresponding author. Department of Materials Engineering, KU Leuven, Leuven, 3001, Belgium.
** Corresponding author.
*** Corresponding authors.
**** Corresponding author. Biorefining and Advanced Materials Research Center, SRUC, Edinburgh, EH9 3JG, United Kingdom.
E-mail addresses: ning.han@kuleuven.be (N. Han), cao-yue@foxmail.com (Y. Cao), a_gang@sdut.edu.cn (F. Wang), Vijay.Thakur@sruc.ac.uk (V.K. Thakur).
[1] Qing Wang and Ning Han are co-first authors.

https://doi.org/10.1016/j.nanoms.2022.07.003
Received 2 June 2022; Accepted 7 July 2022
Available online xxxx

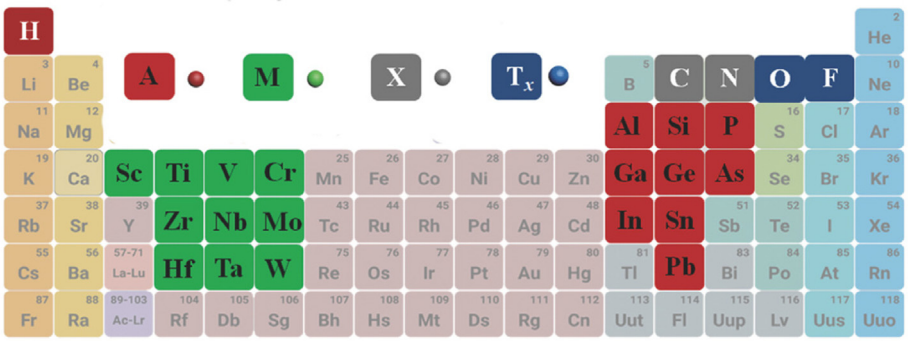

Fig. 1. The main element that forms the MAX phase [40].

familiar with, the functional groups on the surface of MXene have better compatibility with other substrates through chemical bonding force. Carbon nanotubes have hard structures and smooth surfaces, making it difficult to form stable suspensions. In addition, the negative effect of the ultra-high modulus obviously hinders the atomic motion in the internal microstructure, and the internal atomic structure of graphene and carbon nanotubes exacerbates the difficulty of meeting the requirements of high-sensitivity sensors [16–18]. Metal nanowires and nanosheets also occur the same flocculation problem. Conductive polymers are promising sensor candidates [19]. However, there are so many types of conducting polymers that it can be difficult to determine which is the focus for sensing applications. Due to the Because of the excellent properties of MXene, its application field and scale have reached a new level [20–23].

From the current overall point of view, the main issues focus on achieving an sensor compatible with excellent sensitivity, cycle stability, detection range, detection limit, and ultra-low response time [24–30]. Electrode modification is one of the most effective methods to improve the performance of electrochemical sensors. The sensitivity, detection limit, adhesion, selectivity, and dynamic range of electrochemical sensors both can be optimized and improved. For these reasons, electrochemical sensors based on nanomaterials have got significant attention over the past several years to detect various analytes [31–34]. Two-dimensional nanomaterials, such as graphene [35–37] and molybdenum disulfide [38,39], have been extensively researched to build sensitive sensing platforms, either alone or in the form of nanocomposites. However, 2D materials also have their corresponding disadvantages, such as the low conductivity and high hydrophobicity of molybdenum disulfide, the high hydrophobicity of graphene, and the difficulty of functionalizing the surface. Surface functionalization of graphene can only occur at surface defects and edges, and molybdenum disulfide is even more difficult to functionalize its surface. In addition, mass production of this material is a slow and cumbersome process, which further limits the growth of this field. MXenes have excellent electrical conductivity, abundant surface functional groups, easy functionalization, high hydrophilicity, good ion intercalation properties, and easy mass production, making it an ideal choice for building electrochemical sensors with high performance.

The quantity of papers on MXene-based sensors are increase every day. A systematic summary of the preparation methods, properties and applications is necessary. In recent years, many research papers on MXene-based sensors have been published, but they covers different applications and various types. Therefore, it is necessary to give an overview of the progress and prospects in the domain of MXene-based sensors. This paper starts with various synthesis of MXene, and summarizes the latest research results of electrochemical biosensors based on MXene, including preparation methods, sensing properties and application prospects for different detection substances. Finally, we convey our opinions on the prospects and evolution challenges of the new, rapidly developing and promising field of MXene based sensors.

2. Preparation of MXenes

Since the first synthesis of MXene by Naguib et al., in 2011, various types of MXenes have been discovered. In general, MXenes can be obtained by removing the A layer and exfoliating the MAX phase (Fig. 2A). As the precursor to MXenes, the MAX phase is usually a series of layered ternary compounds, where M is the transition metal (i.e. Sc, Ti, V, Cr, Zr, Hf, Nb, Mo, Ta, and W), A is an element of the IIIA or IVA groups in the periodic table (usually Al or Ga), and X is carbon or nitrogen. The MAX phases are P63/MMC symmetric layered hexagon, where the M layer is nearly closed, and the X atoms fill the octahedral positions [8]. The $M_{n+1}X_n$ layers interlace in turn with the A atomic layers [41]. The strong M-X bonds have covalent/metal/ion mixing characteristics, while M-A bonds are metal [42,43]. Unlike with other layered materials such as graphite and transition metal dichalcogenides, where weak van der Waals interactions hold the structure together, the bonds between the layers of the MAX phase are too strong to be broken by shear or any similar mechanical means [44]. The A layer can be chemically selectively etched without breaking the M-X bond by taking advantage of differences in properties and relative strength between M-A and M-X bonds [8]. So far, the synthesis methods of MXenes have been relatively mature. The following will briefly introduce the research status of MXenes synthesis.

2.1. Acid etching method

Using HF to etch Ti_3AlC_2MAX phases was first proposed by Naguib et al., in 2011 years [1]. A substitution reaction with hydrofluoric acid removes the aluminium layer in the Ti_3AlC_2 MAX phase, and hydrogen is produced at the same time. The deionised water and HF solution will also take a reaction that produced Ti_3C_2 to obtain $Ti_3C_2T_x$ while producing hydrogen as well. A range of MAX compounds, involving Ti_2AlC [45], Nb_2AlC [46], Ti_3SiC_2 [47], Mo_2Ga_2C [48] and $Zr_3Al_3C_5$ [49], are also separated into MXenes by this way.

It was subsequently found that a combination of fluoride salts (NH_4HF_2 [50], LiF [51], NaF, KF [52], and FeF_3 [53], etc.) and hydrochloric acid could replace the direct use of hydrofluoric acid. This method is also known as in situ hydrofluoric acid etching(as shown in Fig. 2B), producing 3-5 wt% of HF etching solution. For MXenes synthesized by the method of in situ HF generation, due to the intercalation of cations and water molecules, the layer spacing is increased, and the interlayer force between layers is decreased, the subsequent use of ultrasound can make the material more easily stratified. This method is milder than the direct use of hydrofluoric acid and is usually used to prepare a single or few layers of MXenes. It should be noted that the time and power of ultrasound should be controlled when obtaining single or small layers with ultrasound. The high power and long ultrasound will lead to excessive MXenes laminates and produce unnecessary defects [54].

The use of water as the main solvent is what these etching methods have in common, making the application of MXenes limited. Michel W.

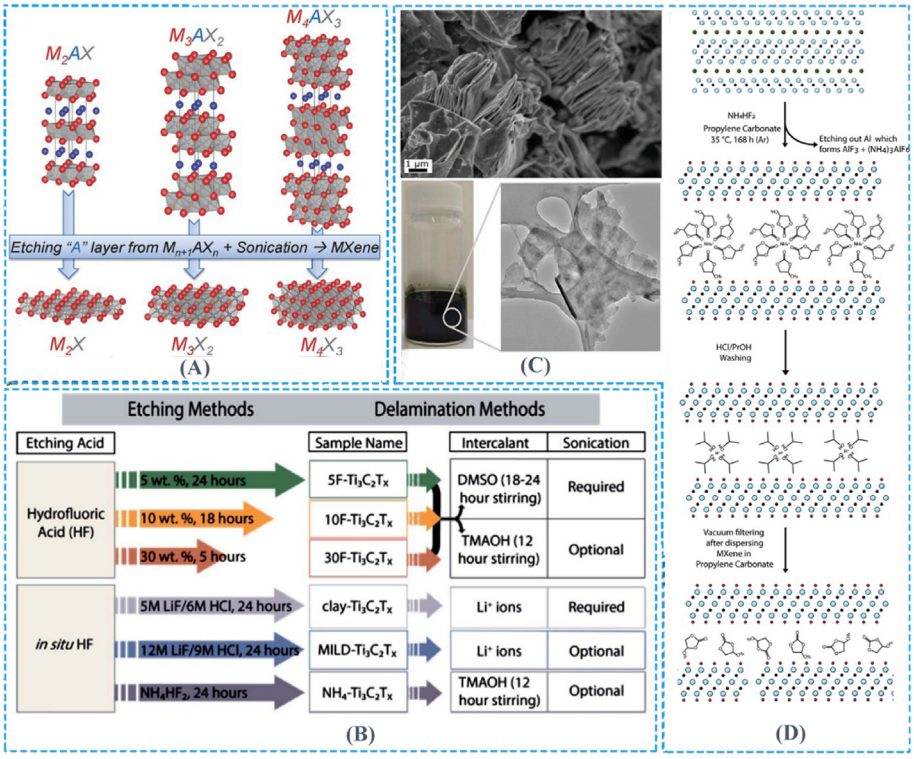

Fig. 2. **(A)** Structure of MAX phases and the corresponding MXenes [8]. **(B)** Synthesis map for $Ti_3C_2T_x$ nanosheets [54]. **(C)** SEM micrograph of $Ti_3C_2T_x$ sample and TEM micrographs of delaminated sheets; **(D)** Schematic of etching and washing steps [55].

Barsoum et al. demonstrated an etch and stratification of Ti_3AlC_2 using an organic polar solvent containing ammonium hydrogen fluoride (NH_4HF_2) instead of using water as the solvent(see Fig. 2D) [55–58]. Further studies showed that fluorine-rich $Ti_3C_2T_x$ flakes could be obtained using this etching method. The authors demonstrated that Ti_3AlC_2 could be etched and stratified using an organic solvent containing NH_4HF_2 without the presence of water(see Fig. 2C).

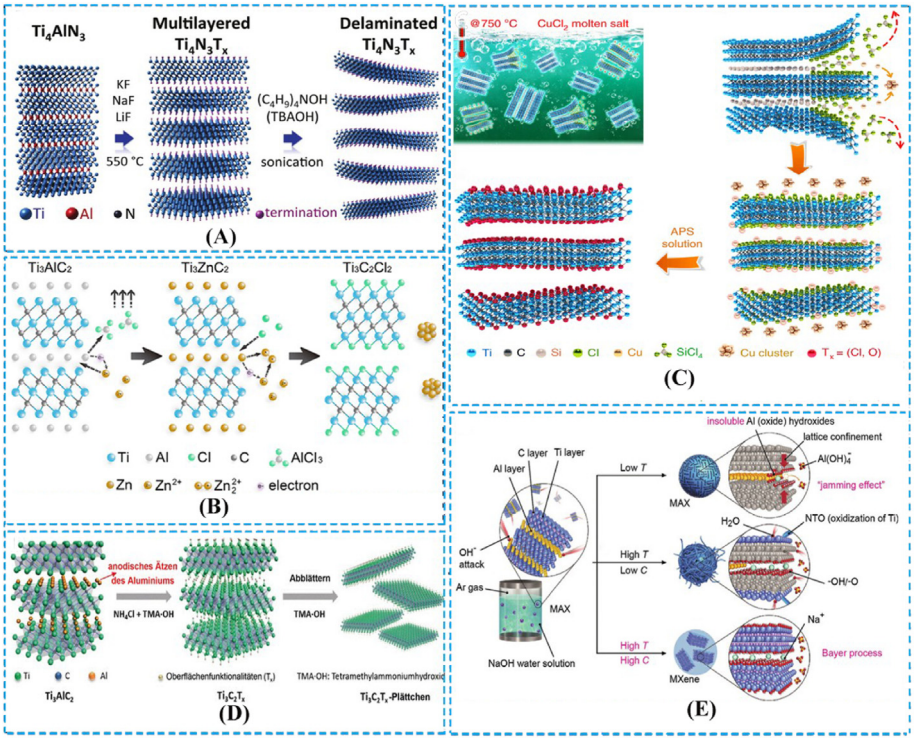

Fig. 3. **(A)** Schematic of synthesize the Ti_4N_3Tx with molten salt method [59]. **(B)** Element replacement in molten salt to synthesize MAX and MXenes [63]. **(C)** The etching process of Ti_3C_2 prepared by dipping Ti_3SiC_2 in $CuCl_2$ molten salt [68]. **(D)** Schematic diagram of anodic corrosion and lamination of Ti_3AlC_2 in binary aqueous solution [70]. **(E)** Reaction of Ti_3AlC_2 with NaOH aqueous solution under different conditions [71].

2.2. Molten salt etching method

Recently years, synthesising MXenes by Lewis acid molten salt has also attracted much attention. Urbankowsk et al. report on synthesising the first 2D transition metal nitride, Ti_4N_3-based MXene. They successfully removed Al from the structure by mixing fluoride salt (KF:LiF:NaF = 59:29:12) and Ti_4AlN_3 powder at a mass of 1:1, heated to 550 °C for 30 min in an argon atmosphere and obtained 2D Ti_4N_3 [59]. The synthesis process is schematically shown in Fig. 3A. Nitride MXenes are predicted to have various attractive properties, like ferromagnetism and higher electrical conductivity than carbide or semiconductor properties [60–62].

The Huang Qing's team successfully synthesized various new MAX phases and MXenes in ZnCl2 molten salt by element replacement (see Fig. 3B) [63]. In the molten state, $ZnCl_2$ is the so-called Lewis acid [64]. The content of $ZnCl_2$ in the reaction is critical. When the molar ratio of Al-MAX to $ZnCl_2$ is 1:1.5, the Zn-MAX phase is mainly formed, and when the molar ratio of Al-MAX to $ZnCl_2$ is 1:6, the chemical reaction time of melting is controlled to generate Cl-MXenes and metallic zinc by-products. Some of the remaining side-reaction impurities are removed by washing with dilute hydrochloric acid, leaving the functional groups with Cl and O MXenes. It is worth noting that this is the Cl-terminated MXenes obtained by non-fluorine chemical methods, and the detailed synthesis method can be found in Refs. [63,65–67].

Li et al. successfully extended the molten salt stripping strategy to various chloride Lewis acid molten salts ($ZnCl_2$, $FeCl_2$, $CuCl_2$, AgCl, etc.) and more members of the MAX phase family (such as Al, Zn, Si, Ga, etc.) [68]. Using direct redox coupling between the A element and the cations of Lewis acid molten salts, they proposed a general method of etching the MAX phase. Fig. 3C illustrates the etching process of Ti_3C_2 prepared by dipping Ti_3SiC_2 in $CuCl_2$ molten salt. In non-aqueous electrolytes, the MXenes exhibit a high rate capability and high storage capacity of lithium, thus making them promising electrode materials for high-rate batteries and hybrid systems. Through this Lewis acid etching process, a broader selection of MAX phase precursors is available for the synthesis of new MXenes. In addition, the Lewis acid etching process of MXene materials offers unprecedented opportunities for surface chemistry and performance tuning.

Through substitution and elimination reactions, Dmitri V. Talapin's research group [69] using the Lewis acid molten salt method and successfully synthesized MXene with Cl, S, O, Te, Se, NH, and Br surface terminals, and no surface MXene of the terminal. So far, the surface functional groups of MXenes have more choices, involving F, Cl, Br, O, S, Se, Te, and other groups. The design and preparation of specific functional groups MXenes can give MXenes special surface chemistry, structure, and properties.

2.3. Other preparation methods

In addition to the above-mentioned acid etching method and molten salt method, there are also some methods such as electrochemical anode etching method, alkaline etching method, chemical vapour deposition method, in-situ electrochemical synthesis method, etc. It is worth mentioning that the latter several methods are fluorine-free preparation of MXenes, which we will introduce individually in this subsection.

2.3.1. Anodic corrosion method

Yang et al., in 2018 [70] demonstrated an efficient fluorine-free corrosion method based on anodic corrosion of titanium-aluminium carbides in binary aqueous solutions. By dissolving aluminium and then replacing it with hydroxyl, ammonium hydroxide is intercalated in situ (Fig. 3D), forming single or double layer flakes with a large average size and high yield (>90%). There is no F involved in the whole process, and the $Ti_3C_2T_x$ sheet does not contain F groups.

2.3.2. Alkaline etching method

An economical approach is to dissolve the A layer in MAX by using a high temperature as well as high concentration NaOH solution to obtain multilayer $Ti_3C_2T_x$(T = O, OH) of up to 92%(mass fraction) [71]. This method is also fluorine-free. As a result of synthesising the Ti_3C_2 layer at high temperature and alkali concentration, the surface is filled with = O and –OH groups. As a result of the high temperature and alkali concentration, $Ti_3C_2T_x$ is formed (see Fig. 3E). Low amounts of water and high temperatures will prevent the titanium layer from oxidizing.

2.3.3. Chemical vapour deposition method

Additionally to the above methods, some researchers have reported the preparation of 2D ultra-thin α-Mo_2C crystals with a large area of high quality by chemical vapour deposition (CVD) [72]. The carbon source for this experiment is methane, while the substrate is copper foil. Then high-quality 2D ultra-thin α-Mo_2C crystals with a thickness of several nanometers and a transverse size of over 100 μm were grown at temperatures above 1085 °C. For specific methods, see Ref. [72]. The two-dimensional MXenes are synthesized by a combination of chemical vapour deposition and physical vapour deposition, and high-quality (defect-free) large monolayer crystals and bare MXenes can be prepared. These materials will contribute to the research of basic physical (quantum) properties and electronic applications in bioelectronics, artificial electrochemical synapses, or neuromorphic computing [73].

2.3.4. In situ electrochemical method

The Chunyi Zhi and Qing Huang's team proposed an integrated solution based on a V_2CT_x MXene zinc ion battery. By using in situ electrochemical routes, using MAX as the positive electrode and F-rich electrolyte as the corrosive, V_2CT_x based zinc ion battery is directly prepared. The Al layer in MAX is gradually removed by electrochemical cycling process, and the MXenes flakes are obtained in situ at the electrode [74]. After etching, the entire battery system can continue to work as usual, and the resulting MXene sheet layer directly serves as a new generation of active materials to show more excellent electrochemical performance. This study proposes a new green method to synthesize MXenes.

Different synthesis methods have different surface functional group structures. For example, reducing the degree of oxidation of MXene with water-free etchants can improve its chemical stability. The defects will be reduced by eliminating fluorine-containing etchants from MXene, and adjustable termination should be achieved. Among the various etching techniques that have been developed, increasing the yield of MXene products by wet etching the MAX phase in acidic fluoride solutions is still the preferred technique for mass production [73].

3. MXenes applied in sensor

In this section, we discuss the application of electrochemical sensors made from MXenes materials to detect biomarkers, drugs, and environmental pollutants. It discusses the fabrication process, electrochemical response, and applications of the sensor, as well as the electrochemical properties of the sensor (limit of detection, range of detection, sensitivity, stability, etc.). Table 1 summarizes MXene-based electrochemical sensors for the detection of different analytes.

3.1. Detecting biomarkers

The biomarker is a biomolecule found in blood, body fluids, and tissues that can be detected as a marker of normal/abnormal biological processes and pathogenic conditions/diseases [96]. Biomarkers can be identified by non-invasive methods in tissue samples (surgical removal) and body fluids (blood, urine). Proteins, nucleic acids, isozymes, hormones or metabolites, etc. can all be one of the biomarkers. Changes in the amount or level of a particular biomarker in cells usually indicate disease progression [97]. For better early diagnosis of disease and monitoring of disease progression, specific identification of biomarkers can be used to detect their level status [98–100]. Traditional biomarker

Table 1
MXene-based electrochemical sensors for the detection of different analytes.

Electrode	Analyte	Detection range	Detection limit	Reference
NiO/$Ti_3C_2T_x$	H_2O_2	0.01–4.5 mM	0.34 μM	[75]
Nafion/Hb/Ti_3C_2/GCE	H_2O_2	0.1–260 μM	20 nM	[76]
Nafion/Hb/TiO_2–Ti_3C_2/GCE	H_2O_2	0.1–380 mM	14 nM	[77]
$Ti_3C_2T_x$/GCE	H_2O_2	–	0.7 nM	[78]
$Ti_3C_2T_x$/PtNP/GCE	H_2O_2	490 μM ~ 53.6 mM	448 nM	[79]
MXene-Ti_3C_2/GOD	Glucose	39.8 μM ~ 1.319 mM	1.96 μM	[80]
MXene/NiCo-LDH/GCE	Glucose	2 μM ~ 4.096 mM	0.53 μM	[81]
Ti_3C_2–HF/TBA/GOx/GTA	Glucose	50–27750 μM	23 μm	[82]
Chit/ChOx/$Ti_3C_2T_x$/GCE	Cholesterol	0.3–4.5 nM	0.11 nM	[83]
$Ti_3C_2T_x$ MXene/GCE	H_2S	0.1–300 μM	16 nM	[84]
TDN/MXenes	Gliotoxin	5 pM ~ 10 nM	5 pM	[85]
$Ti_3C_2T_x$/GCE	Dopamine	0.015–10 μM	3 nM	[86]
MIP/K^+-$Ti_3C_2T_x$/GCE	Triclosan	10 nM–50 μM	1.18 nM	[87]
MXene@AgNC/NH_2-MWCNTs/GCE	Carbendazim	0.3 nM–10 μM	0.1 nM	[88]
MXene/ERGO/GCE	Carbendazim	2 nM ~ 10 μM	0.67 nM	[89]
AChE/Ag@$Ti_3C_2T_x$	Organophosphorus pesticides	10^{-14}–10^{-8} M	3.27 × 10^{-15} M	[90]
MXene/ZIF-67/CNTs/GCE	Luteolin	0.1 nM–1 μM	0.03 nM	[91]
$Ti_3C_2T_x$-ZIF-8/GCE	Hydrazine	10 μM ~ 7.7 mM	5.1 μM	[92]
Nafion/Hb/MXene-Ti_3C_2/GCE	Nitrite	0.5 μM–11.8 mM	0.12 μM	[93]
alk-Ti_3C_2/GCE	Cd(II), Pb(II), Cu(II), Hg(II)	0.1–1.5 μM	98 nM, 41 nM, 32 nM, 0.13 μM	[94]
H–C_3N_4/$Ti_3C_2T_x$	Cd^{2+}, Pb^{2+}	50 nM ~ 1.5 μM, 50 nM ~ 1.5 μM	1 nM, 0.6 nM	[95]

detection methodshave the technical limitations of slow detection speed and the consumption of costly reagents for each detection [101,102]. Additionally, these traditional means of continuous monitoring of patients during treatment are not ideal. Furthermore, all diseases are multifactorial, not just involving a molecule or substance in a cell. Therefore, the detection of multiple biomarkers simultaneously and the correct detection results are critical for diagnosis [103–105]. Clinical diagnostics focus on developing analytical techniques that enable sensitive and parallel detection of biomarkers to provide functional point-of-care testing. For several years, there has been a increased attraction in biosensors' development due to biosensors' excellent analytical performance and measurement in real-time. They can detect lower levels of biomarkers in physiological samples that can aid in the early diagnosis of disease. They enable biorecognition molecules to be reused, avoiding time delays in sample analysis. In addition, electrochemical biosensors have good selectivity and can detect multiple biomarkers simultaneously, which has shown great potential. This chapter, we summarize the recent design and fabrication methods and sensing performance of MXene-based electrochemical biosensors to detect biomarkers.

3.1.1. H_2O_2 sensor

Hydrogen peroxide (H_2O_2) has good oxidizing and reducing properties and is widely used in food production, medical, clinical, and chemical industries. In living cells, H_2O_2 is a by-product of various oxidase reactions and plays a vital role in biological systems [76,106–109]. Hence, readily available, low-cost, and reliable analytical methods for the detection of H_2O_2 are essential. Ramachandran et al. prepared NiO/-$Ti_3C_2T_x$ microsphere porous structures by calcining Ni-MOF/$Ti_3C_2T_x$ and applied them to electrochemical sensing of H_2O_2 [75]. The NiO attached to the $Ti_3C_2T_x$ surface can prevent the accumulation of MXene sheets. The addition of the $Ti_3C_2T_x$ sheets effectively enhances the mesoporous structure due to interlayer voids and can maximize the accessibility of NiO. The NiO/$Ti_3C_2T_x$ sensor shows a low limit of detection of 0.34 μM and a wider linear range of 0.01–4.5 mM. More electroactive sites for electrochemical redox reactions on H_2O_2 sensing are available thanks to increased NiO/$Ti_3C_2T_x$'s specific surface area and porosity. In addition, $Ti_3C_2T_x$ prevents leaching and scaling effects in the three-dimensional porous network. It facilitates the uncomplicated access of electrolyte ions to the electrode surface, enhancing the efficient electron transport, and improving electrochemical applications.

Wang et al. immobilized hemoglobin (Hb) on the surface of a multilayer accordion-like Ti_3C_2 material to prepare a medium-free biosensor for detecting H_2O_2. MXene-Ti_3C_2 has a favorable enzyme immobilization ability [76]. The prepared biosensor has good detection performance for H_2O_2, the linear range for H_2O_2 is 0.1–260 μM, and the lower detection limit for H_2O_2 is 20 nM. In addition, Wang et al. synthesized TiO_2 nanoparticles-modified Ti_3C_2 MXene nanocomposites via in situ hydrolysis and hydrothermal processes, and used them to prepare a mediator-free biosensor for hydrogen peroxide detection [77]. As shown in Fig. 4A, a large amount of TiO_2 nanoparticles supported on Ti_3C_2 layered substrates endow the nanocomposites with many advantages when used as enzyme immobilization carriers. Fig. 4B is the SEM image of TiO_2–Ti_3C_2 nanocomposite. The organ-like structure of the Ti_3C_2 nanolayer closed at one end and open at the other end facilitates the encapsulation of enzymes. The enzyme was funneled inwardly between Ti_3C_2 nanolayers and could be fixed on the inside surface of organ-like structures. In addition, nano-titanium dioxide with strong biocompatibility can offer a protective microenvironment for the enzyme, allowing it to maintain its stability and function over time. The adsorbable active surface area of proteins can be significantly increased using nanoscale titanium dioxide. At the same time, the substrate can be wrapped in a hybrid structure with a large specific surface area, allowing for the immobilization of a large number of enzymes on the nanocomposite. In this confined region, the practical collision between the substrate and enzyme will be increased due to the concentrated substrate and enzyme. Ti_3C_2 has good carrier mobility and can also be a good medium for efficient electrical communication between enzymes and electrodes. The biosensor has a lower detection limit of 14 nM for H_2O_2, a linear range of 0.1–380 mM for H_2O_2 (Fig. 4C), and good long-term stability due to the reasons mentioned above. This research shows that TiO_2–Ti_3C_2 nanocomposites could be used as biocompatible platforms for enzyme immobilization and direct electrochemical biosensor fabrication.

In another report, Lenka et al. developed the $Ti_3C_2T_x$/GCE nonenzymatic sensor to detect H_2O_2 down to nanomolar range with a fast response time less than 10 s [78]. The detection limit of the sensor is 0.7 nM and the sensitivity is 596 $mAcm^{-2}mM^{-1}$. The prepared $Ti_3C_2T_x$ sensor is more sensitive to detecting H_2O_2 than reported previously. It is a simple and efficient method to make a non-enzymatic H_2O_2 biosensor with high sensitivity and a low limit of detection, which can reach the nanomolar level. In addition, Lenka et al. also investigated the electrochemical performance of platinum nanoparticles (PtNPs) modified 2D $Ti_3C_2T_x$ thin films [79]. The outcomes demonstrated that the $Ti_3C_2T_x$/PtNP nanocomposites coated on the GCE surface exhibited better and more stable redox behavior than the unmodified $Ti_3C_2T_x$/PtNP nanocomposites within the anodic potential window. For instance, this H_2O_2 sensor of $Ti_3C_2T_x$/PtNP-modified GCE has a limit of

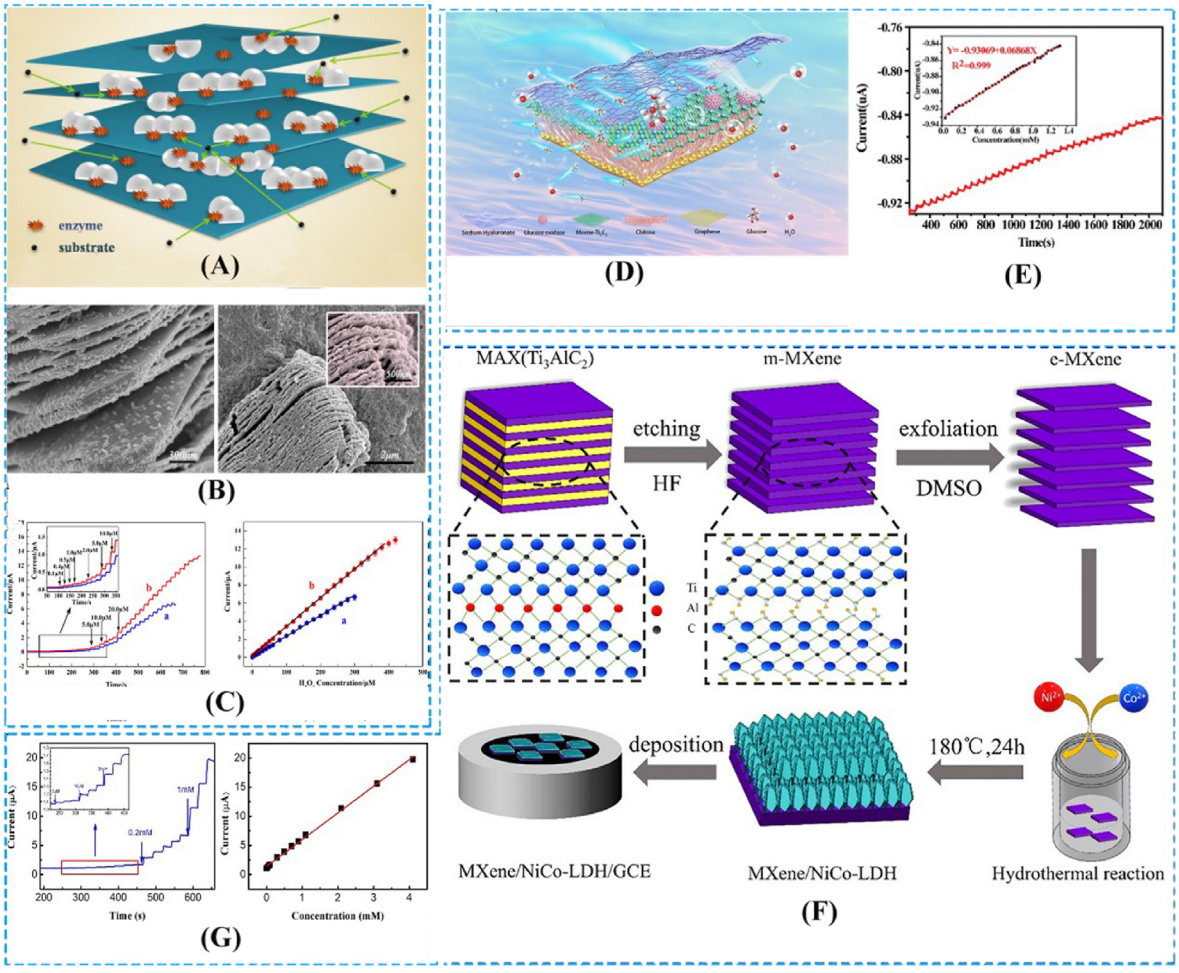

Fig. 4. **(A)** Schematic diagram of TiO_2–Ti_3C_2 complex hemoglobin. **(B)** SEM images of TiO_2–Ti_3C_2 nanocomposite and Nafion/Hb/TiO_2–Ti_3C_2 composite film. **(C)** Current-time response of continuous addition of H_2O_2 and relationship between steady-state current and H_2O_2 concentration [77]. **(D)** Schematic diagram of the structure of the glucose oxidase biosensor. **(E)** Current-time response of continuous addition of H_2O_2glucose [80]. **(F)** The fabrication progress of MXene/NiCo-LDH/GCE. **(G)** Current response of MXene/NiCo-LDH/GCE sensor versus glucose concentration [81].

detection of 448 nM and a reduction onset potential of +250 mV (vs. Ag/AgCl), while the detection limit and reduction onset potential of $Ti_3C_2T_x$-modified GCE are 883 nM and −160 mV, respectively. Electrochemical studies show that the $Ti_3C_2T_x$/PtNP nanocomposites exhibit better redox stability in the anodic potential window than $Ti_3C_2T_x$-deposited GCEs, which is an essential property for further $Ti_3C_2T_x$ Mxene-based sensor development. GCEs modified with $Ti_3C_2T_x$/PtNP can detect H_2O_2 under an optimum potential range with a limit of detection of 0.448 μM. In addition, other tiny organic molecules (dopamine, ascorbic acid, uric acid, and acetaminophen) were also studied for their redox properties. These substances can be identified at higher potentials than H_2O_2, with LODs lower or equivalent to previously reported values, enabling this interface to be advantageous for various sensing applications.

3.1.2. *Glucose sensor*

Electrochemical enzymatic sensors have gotten a lot of attention because of their unique selectivity, quick reaction, low cost, and ease of downsizing [110–113]. Due to enzymes' instability and ease of deactivation, there are few electrochemical enzyme sensors with practical applications. As we all know, immobilized enzymes possess the relatively high activity and stability than free enzymes. Gao et al. proposed a strategy to construct a novel enzymatic sensor for detecting glucose [80]. As depicted in Fig. 4D, sodium hyaluronate (SH) acts as a permeable protective membrane to shield the enzyme from contamination and dehydration, facilitating glucose diffusion towards the sensor interface. MXene-Ti_3C_2 and glucose oxidase (GOD) composed the reaction layer, and MXene-Ti_3C_2 can provide a highly scattered glucose oxidase loading. The adhesion layer is composed of chitosan and reduced graphene oxide (rGO). Chitosan helps to organically combine MXene-Ti_3C_2 with rGO and ensures the high biocompatibility of the sensor. During the reaction, the permeable protective membrane allows glucose to swiftly pass through and enter the reaction layer (MXene-Ti_3C_2/GOD) to react on the GOD surface. The rGO-decorated collector enables rapid release and efficient collection of electrons. For glucose sample detection, this sensor with a linear response from 39.8 μM to 1.319 mM and a limit of detection of 1.96 μM (Fig. 4E). This study provides new ideas for developing stable and reliable enzymatic biosensors and broadens its application fields.

In addition to enzymatic sensors, non-enzymatic sensors will then be introduced. Li et al. in situ synthesized 3D porous NiCo-LDH nanosheets on MXene (Ti_3C_2) by hydrothermal method (Fig. 4F) and explored the glucose sensing performance of MXene/NiCo-LDH nanocomposites [81]. As shown in Fig. 4G, the current response of MXene/NiCo-LDH/GCE exhibited a linear relationship from 2 μM to 4.096 mM, and the sensitivity of this electrode is 64.75 μA mM^{-1} cm^{-2} and the detection limit is 0.53 μM. The MXene/NiCo-LDH/GCE exhibits low limit of detection and fast current response to the oxidation of glucose, which is due to the synergistic effect of the large specific surface area, rapid electron transfer rate, and effortless electrolyte diffusion of the MXene/NiCo-LDH composite.

Chia et al. investigated the heterogeneous electron transfer capability of Ti_3C_2 fabricate by hydrofluoric acid etching and subsequently layered with TBAOH to develop a glucose biosensor [82]. As shown in Fig. 5A, MXene and glucose oxidase were sequentially added to the surface of the glassy carbon electrode, and then cross-linked with glutaraldehyde to prepare the glucose biosensor. This MXene-based biosensor can detect glucose selectively, sensitively, and quickly. Chronoamperometry indicates that the sensor shows excellent selectivity to detect glucose, with a linear range of 50–27750 μM and a lower detection limit of 23.0 μm (Fig. 5B and C). This study provides a proof of concept for possible future applications of pristine MXenes to develop electrochemical biosensors with excellent selectivity and sensitivity for biomedical and food sampling applications.

3.1.3. Cholesterol sensor

Cholesterol is an important lipid in the human body, a major component of cell membranes, assisting in the maintenance of cell membrane permeability and fluidity. Cholesterol is a key biomarker for a variety of diseases [114–116]. Hypolipoproteinemia, malnutrition, sepsis, malnutrition, and anemia can all be caused by low cholesterol levels [117]. The usual range for maintaining cholesterol levels in the body is 2.83–5.20 mM [118]. As a result, in the academic and medical fields, accurate, sensitive method to monitor cholesterol levels is required. Xia et al. prepared $Ti_3C_2T_x$ by etching Ti_3AlC_2 with HF and LiF [83]. The synthesized $Ti_3C_2T_x$ has high specific surface area, biocompatibility, good electrical conductivity and dispersibility, all of which contribute to electron transport. Subsequently, using a continuous self-assembly approach to prepare Chitosan(Chit)/Cholesterol Oxidase(ChOx)/$Ti_3C_2T_x$ nanocomposites. The scanning electron microscope images of Chit/ChOx/$Ti_3C_2T_x$ are shown in Fig. 5E. Furthermore, adopt a one-step dip coating process to fabricate the biosensor to detect cholesterol(Fig. 5D). Chit and $Ti_3C_2T_x$ are support structures that help to immobilize ChOx enzymes while also increasing conductivity. During cholesterol oxidation, the addition of a redox mediator ($Fe(CN)6^{3-/4-}$) aided electron transfer between the analyte and the electrode. The DPV response showed a rise in current with increasing cholesterol

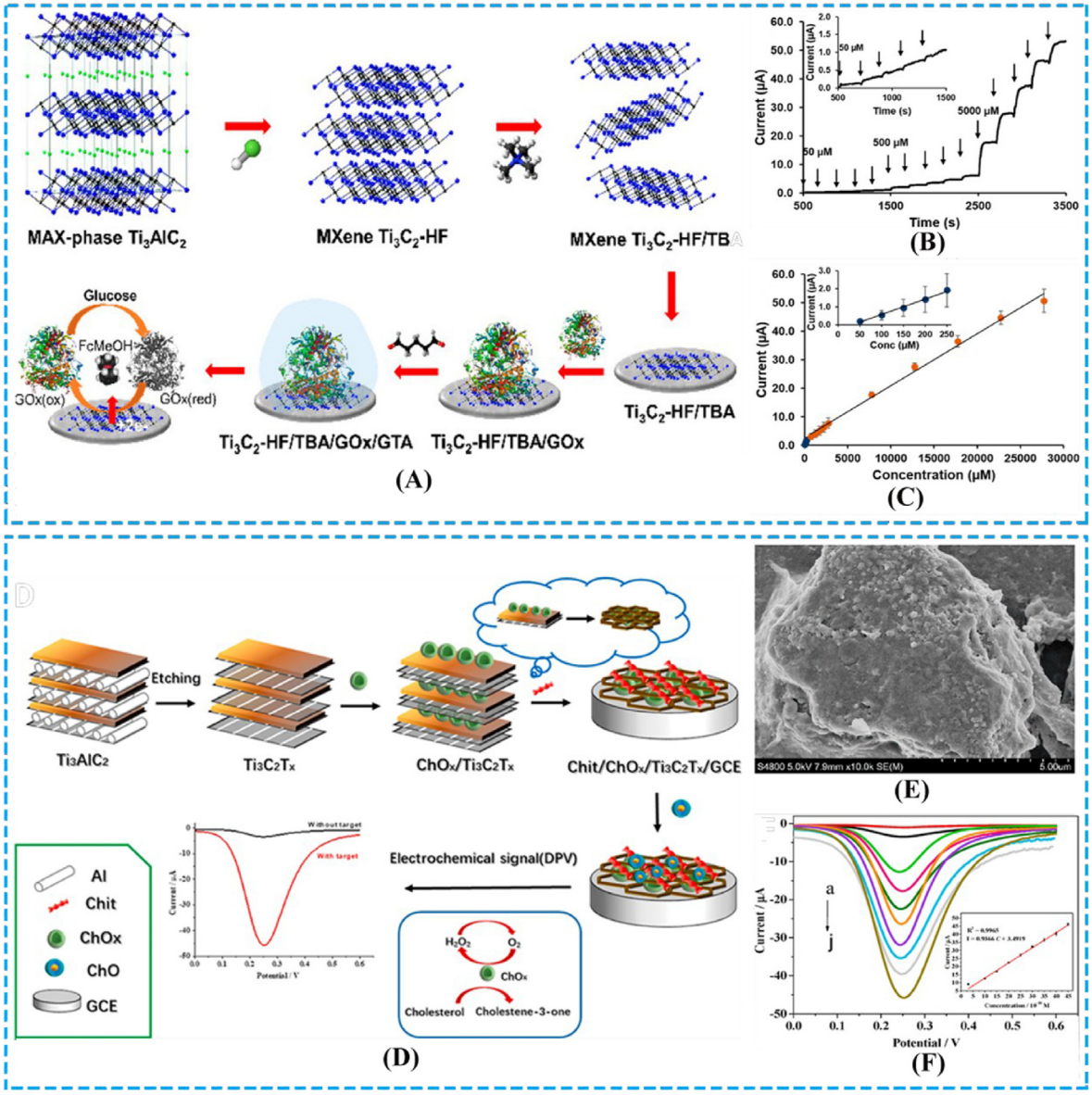

Fig. 5. **(A)** Flow chart for the fabrication of mxene-based glucose sensors. Chronoamperometry **(B)** and calibration plot **(C)** of the Ti_3C_2–HF/TBA-based glucose sensor [82]. **(D)** Preparation process of Chit/ChOx/$Ti_3C_2T_x$/GCE. **(E)** SEM images of MXene and MXene/Chit/ChOx/film. **(F)** Differential pulse voltammetry of the Chit/-ChOx/$Ti_3C_2T_x$/GCE biosensor [83].

concentration. Under optimal conditions, the biosensor's DPV response had a strong linear relationship with cholesterol concentration in the range of 0.3–4.5 nM, with a limit of detect of 0.11 nM (Fig. 5F). Furthermore, due to the excellent selectivity and stability of the electrochemical biosensor, the determination of cholesterol has been carried out in actual samples, proving its application prospect.

3.1.4. H_2S sensor

H_2S is widely distributed in animals and plays a very important role in regulating the body's nerves, regulating blood vessel tension, and reducing metabolism [119–122]. Various methods have been tried to detect endogenous H_2S in living organisms, such as colorimetric, fluorescence, and electrochemical methods. Among them, electrochemical methods have become a hot spot in current sensor research because of their cheap cost, quick response, and ease of operation. Liu et al. directly drop coated the prepared $Ti_3C_2T_x$ dispersion on the surface of the GCE electrode to obtain an electrochemical sensor to detect H_2S [84]. The synthesis schematic is shown in the Fig. 6A. In medicine, the word "hydrogen sulfide" refers to a wide range of free sulfides. For this reason, Liu et al. prepared Na_2S solutions as the supply source of H_2S. After testing and calculation, The range of detection is 0.1–300 μM and the limit of detection is 16.0 nM. Meanwhile, the sensor's detection sensitivity is 0.587 $\mu A \mu M^{-1} cm^{-2}$(Fig. 6B and C). In biological samples, there are also several physiological interfering chemicals that are

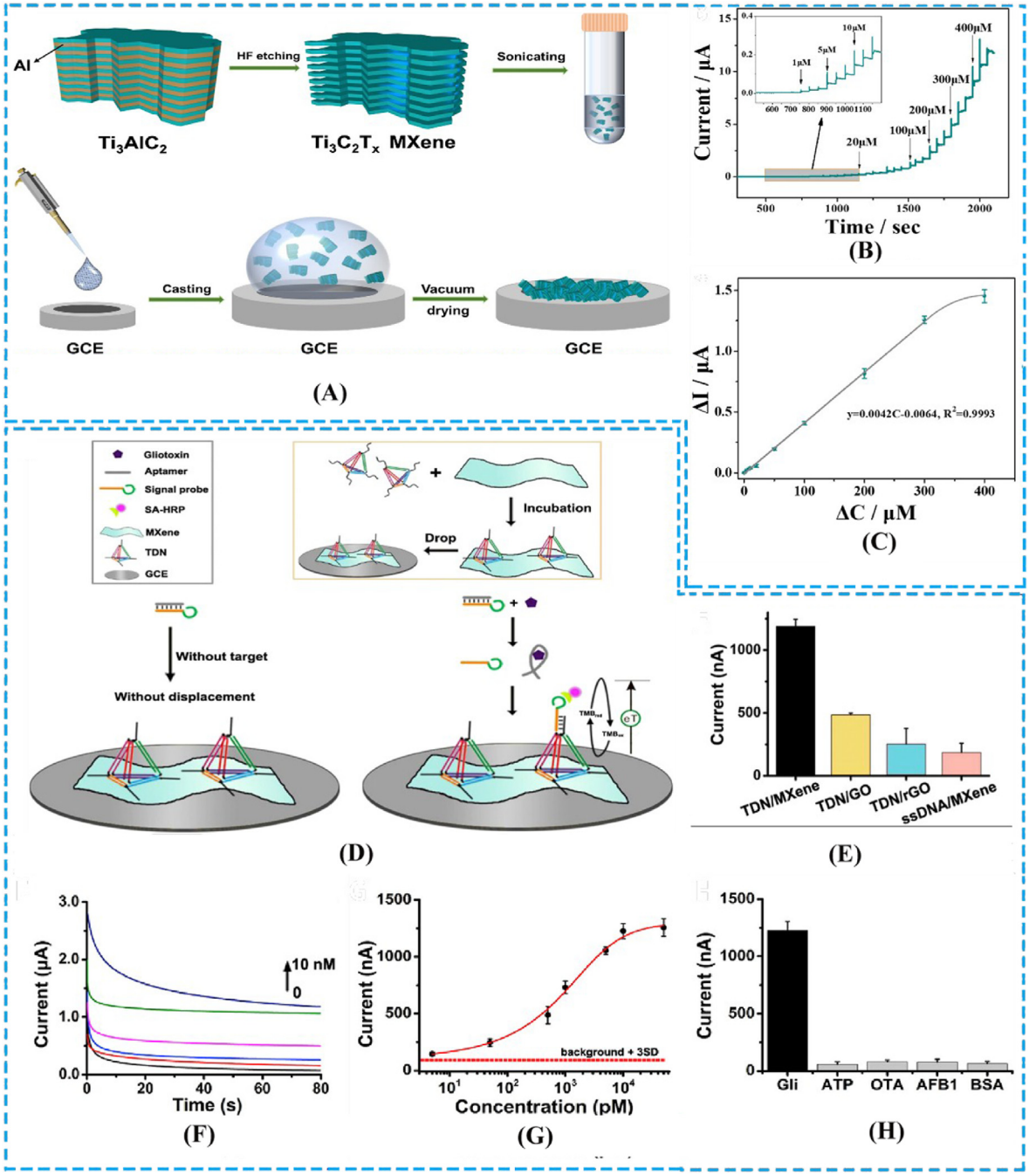

Fig. 6. **(A)** Schematic of synthesis of $Ti_3C_2T_x$ and electrode modification. Current response with different concentration H_2S (B) and calibration curve (C) [84]. **(D)** Schematic diagram of the TDN/MXene gliotoxin electrochemical sensor. **(E)** Comparison of TDN/MXene sensors with other sensors. **(F)** Amperometric curves for the detection of gliotoxin at a series of concentrations. **(G)** Plot of current vs. gliotoxin concentration. **(H)** Selectivity of the gliotoxin sensor [85].

symbiotic with H_2S, such as citric acid, uric acid, L-cysteine, 4-acetate Aminophenol, etc. The results show that the prepared electrodes had little response to 20 μM of other interfering substance. After add 10 μM H_2S, the current increased significantly immediately. That indicates the $Ti_3C_2T_x$/GCE exhibits good selectivity for H_2S. After 28 days, the amperometric response value is 98.84% of the initial value, indicating that the sensing electrode has excellent stability.

3.1.5. Gliotoxins sensor

Gliotoxin is amongst the most poisonous metabolites generated by Aspergillus fumigatus in growing, posing a threat to human and animal health [123]. Wang et al. reported an sensor based on DNA nanostructure-modified MXene (Ti_3C_2) nanosheets to detect gliotoxin [85]. Tetrahedral DNA nanostructures (TDN) are immobilized on the surface of MXene nanosheets through the coordination between phosphate groups on DNA and titanium. Fig. 6D shows the working principle of this electrochemical biosensor. MXene nanosheets can modify a large number of DNA probes due to their high specific surface area. They have high electrical conductivity, which makes electron transport between electrochemical substances and the electrode surface easier (see Fig. 6E). To evaluate the ability of the sensor to detect gliotoxins quantitatively, the researchers tested the I-t decay curves of different concentrations of gliotoxins, and the current increased as the gliotoxin concentration increased from 5 pM to 10 nM(Fig. 6F). As the concentration of gliotoxin increased, the current response reached a plateau point at 50 nM. The limit of detection is 5 pM(Fig. 6G and H). Furthermore, the cost of TDN/MXenes sensor is significantly reduced compared to previous TDN-based electrochemical sensors, which is highly desirable for its scalable applications.

3.1.6. Dopamine sensor

Dopamine (DA) is a neurotransmitter that dopaminergic neurons generate. It functions as a chemical signal in the kidneys, endocrine system, and central nervous system [124–126]. The mean level of DA in human serum is between 0.1 μM and 1 mM, whilst the abnormal DA levels are associated with a variety of neurological diseases [125]. Therefore, we need a sensitive and reliable sensor could detect dopamine in serum. Shahzad et al. developed a DA detection sensor by drop-coating $Ti_3C_2T_x$ solution on the GCE and adding Nafion, which facilitates the firm fixation of $Ti_3C_2T_x$, resulting in the formation of species capable of selectively accumulating positive charges stable film [86]. Previous research has demonstrated that Nafion deprotonates at physiological pH, speculating that the negative charges immobilized on the surface of the MXene sensor electrodes further limit the diffusion of negative charges to the electrodes [127]. Compared with the rGO sensor, the $Ti_3C_2T_x$/GCE sensor exhibits good electrochemical sensitivity to DA, mainly due to the low charge transfer resistance, well intrinsic conductivity, larger specific surface area, and abundant functional groups of $Ti_3C_2T_x$.

3.2. MXene based sensors for pharmaceuticals and pesticides

3.2.1. Triclosan sensor

Triclosan (TCS), namely 5-chloro-2-(2,4-dichlorophenoxy)phenol, is an efficient antibacterial agent, widely used in pharmaceutical preparations, apparel and plastics [128,129]. TCS is a stable lipophilic compound and readily accumulates in organisms and is chronically toxic, posing potential threats to ecosystems and human health [130]. Zhang et al. developed a molecularly imprinted electrochemical sensor (MIECS) based on the $Ti_3C_2T_x$ to detect TCS [87]. $Ti_3C_2T_x$ is used to improve the electrochemical response of MIECS. K^+ are inserted into $Ti_3C_2T_x$ nanosheets, and K^+-$Ti_3C_2T_x$ is formed by soaking in alkaline solution, which improves the sensor's sensitivity. At the same time, the molecularly imprinted polymers(MIP) film is formed by electropolymerization of p-aminobenzoic acid to recognize TCS specifically. The fabrication process of the sensor is shown in Fig. 7A. Under the optimal conditions, the current intensity has an excellent linear relationship with the concentration of TCS (Fig. 7B and C), the linear range is 10 nmol L^{-1}–50 μmol L^{-1}, and the detection limit is 1.18 nmol L^{-1}. Trichlorocarban etc. structural analogs are used as interfering substances to study the selectivity of MIECS. The current responses of MIECS to the four interfering substances are weak, while the current responses of the imprinted electrodes are the largest to TCS (Fig. 7D). This is due to the MIP film's specific cavity modification, which matches the target's spatial structure and binding site. The MIECS combines the benefits of $Ti_3C_2T_x$ and MIP with excellent selectivity and sensitivity, providing a method to fabricate electrochemical sensing platforms with $Ti_3C_2T_x$ and having broad application prospects in the realm of food safety.

3.2.2. Carbendazim sensor

Carbendazim (CBZ) is widely used to prevent and treat fungi-caused crop diseases. However, residues of CBZ have adverse effects on organisms and the environment [131,132]. As a result, developing an effective quantitative detection methods for CBZ residues is critical. Zhong et al. composited MXene@Ag nanoclusters with amino-functionalized multi-walled carbon nanotubes to construct a new ratiometric electrochemical sensor to detect CBZ [88]. Ag nanoclusters (AgNCs) implanted in MXenes can suppress MXene aggregation, increase electrocatalytic activity. Because of the presence of NH_2-MWCNTs, signal amplification was enhanced, and improved sensitivity of the sensor. Depending on this MXene@AgNC/NH_2-MWCNTs composite characteristics, the sensor demonstrates a linear relationship with the concentration of CBZ (0.3 nM–10 μM) and a limit of detection of 0.1 nM(Fig. 7F and G). Furthermore, in the testing of actual samples, the ratiometric electrochemical sensor has great selectivity, repeatability, long-term stability. In another work, Xie et al. combined $Ti_3C_2T_x$ with electrochemically reduced graphene oxide as an electrochemical detection electrode material (MXene/ERGO) for carbendazim [89]. As shown in Fig. 7H, on the electrode surface, a combination of MXene and graphene oxide (GO) was initially dropped, and then GO was electrochemically reduced. Fig. 7I is the SEM image of MXene/ERGO. The ERGO conductive network binds the separation layers of MXene and connects the dispersed MXene particles, thereby enhancing the electrical conductivity, improving the electrochemical reaction performance, and promoting the electron transport from the electrode to the deteced molecule. Therefore, the MXene/ERGO-based sensor shows high sensitivity for detecting CBZ, with a lower detection limit of 0.67 nM (Fig. 7J). The sensor also has outstanding selectivity and repeatability for detecting CBZ and was employed to detect CBZ in vegetables and fruits samples successfully.

3.2.3. Organophosphorus pesticides sensor

Organophosphorus pesticides (OPs) are extensively employed in agriculture to control insect invasion [133]. However, excessive pesticide usage causes pesticide residues to linger in the environment for an extended period of time, thus seriously threatening human health. Jiang et al. prepared Ag@$Ti_3C_2T_x$ nanocomposites by reduction method using MXenes as reducing agent and carrier [90]. Using Ag@$Ti_3C_2T_x$ nanocomposite as support, prepared acetylcholinesterase (AChE) biosensor by drop method to detect OPs. The sensor combines the electrocatalytic properties and synergistic effects of $Ti_3C_2T_x$ nanosheets and Ag nanoparticles, facilitating electron transfer and enlarging the effective area to detect OPs. The electrochemical behavior of the prepared acetylcholinesterase biosensor is tested. The AChE biosensor shows a good detection capability for AChE chloride. The AChE biosensor exhibits linearity in the detection of malathion in the range of 10^{-14}–10^{-8} M, and exhibits excellent selectivity, reproducibility, and stability.

3.2.4. Luteolin sensor

Luteolin (LUT) is a biologically active functional ingredient that has a wide range of pharmacological applications [134–138]. Xu et al. use MXene/ZIF-67/CNTs composites to construct a LUT electrochemical sensor [91]. In the design of the composite material, ZIF-67 was grown on the surface of carbon nanotubes in situ to ensure the stability of its bonding, and then ZIF-67/carbon nanotubes were supported by

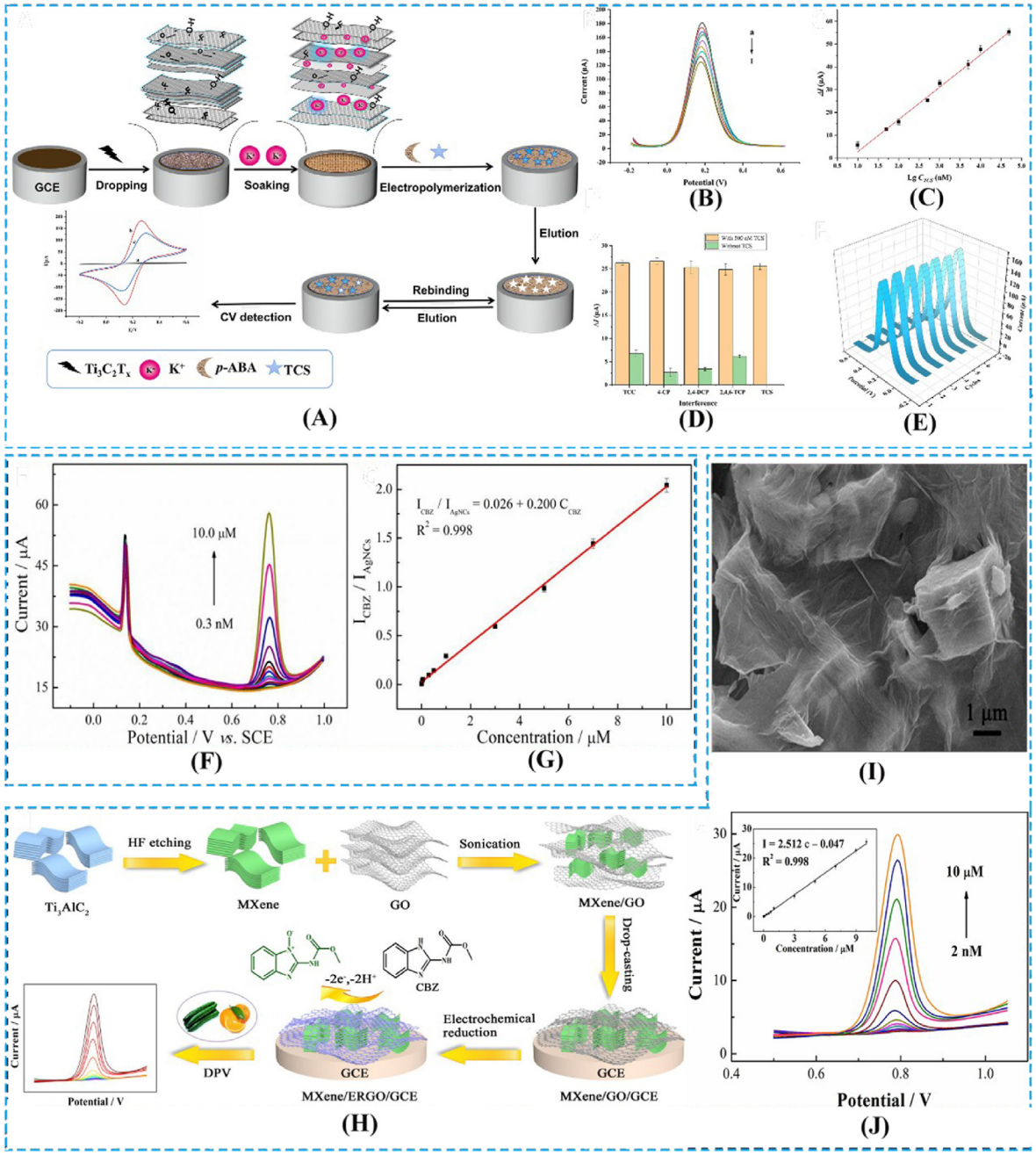

Fig. 7. **(A)** Preparation schematic of MIP/K^+-$Ti_3C_2T_x$/GCE. DPV response curves **(B)**, standard curve of TCS detected **(C)**, selectivity **(D)** and stability **(E)** of MIECS [87]. **(F)** Differential pulse voltammetry curves of MXene@AgNCs/NH_2-MWCNTs/GCE. **(G)** Linear relationship of I_{CBZ}/I_{AgNCs} and CBZ concentration [88]. **(H)** Preparation strategy of MXene/ERGO/GCE sensor. **(I)** The SEM images of MXene/ERGO. **(J)** The differential pulse voltammetry plots of MXene/ERGO/GCE sensor [89].

conductive MXene as a carrier(Fig. 8A shows the preparation process). The MXene/ZIF-67/CNTs sensor exhibited excellent electrocatalytic activity and enhanced current response to LUT redox reaction. By optimizing the experimental parameters, the MXene/ZIF-67/CNTs sensor has excellent performance, showing a good linear relationship in the range of 0.1 nM–1 μM, and a low detection limit of 0.03 nM (Fig. 8B and C). In addition, the MXene/ZIF-67/CNTs sensor exhibits good selectivity, and satisfactory repeatability.

3.3. MXene based sensors for others

3.3.1. Hydrazine sensor

Hydrazine is an essential raw chemical, environmental pollutant, and potent carcinogen. Every year, a considerable amount of hydrazine is released into the environment as a result of misuse and inappropriate treatment [139–141]. So, a fast, accurate, rapid and accurate method for detecting hydrazine is urgently needed. Yao et al. report a way that enhances the conductivity of ZIF-8 by embedding $Ti_3C_2T_x$ [92]. The obtained $Ti_3C_2T_x$/ZIF-8 nanocomposites exhibit valuable analytical performance for hydrazine sensing benefit from the higher electrical conductivity and electrocatalytic activity. The anodic peak current of $Ti_3C_2T_x$-ZIF8/GCE is greatly raised to 30.8 μA in the cyclic voltammetry test, exhibiting high electrocatalytic activity for hydrazine oxidation. MXene's strong conductivity improves peak current responsiveness and allows for quicker electron transport rates. That makes the response current quickly reach a steady state, showing a linear relationship in the

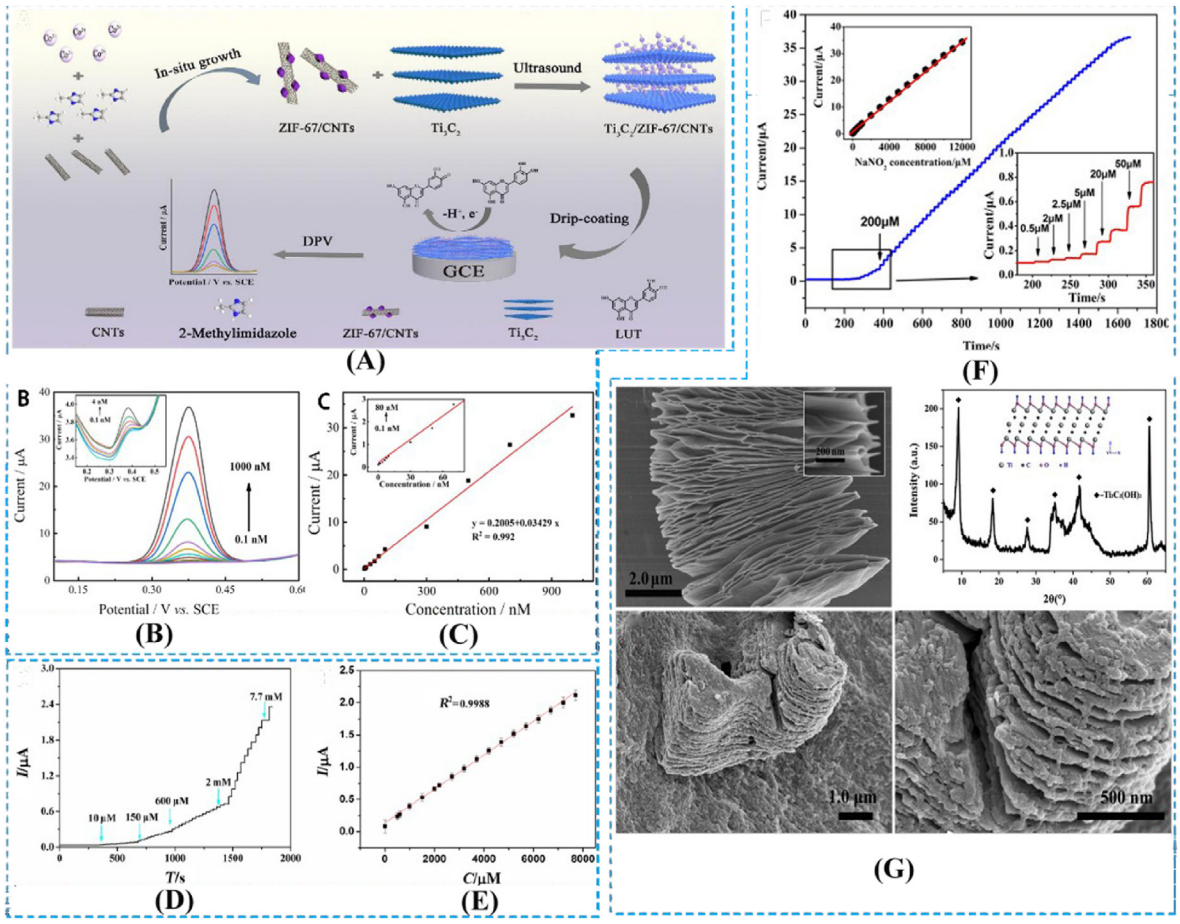

Fig. 8. Schematic diagram of the preparation **(A)**, DPV curves **(B)** of MXene/ZIF-67/CNTs/GCE; **(C)** Linear relationship between peak current and LUT concentration [91]. (D) Calibration plot of response current versus hydrazine concentration for the $Ti_3C_2T_x$/ZIF-8 sensor [92]. **(F)** I-T response curves of Nafion/Hb/MXene--$Ti_3C_2T_x$/GCE sensor with continuous addition of $NaNO_2$. **(G)** SEM images of $Ti_3C_2T_x$ and Nafion/Hb/$Ti_3C_2T_x$ composite film [93].

range of 10 μM–7.7 mM(Fig. 8D and E).

3.3.2. *Nitrite sensor*

As an excellent immobilization carrier, MXene-Ti_3C_2 has good biocompatibility, protein bioactivity and stability [76]. Liu et al. immobilized hemoglobin (Hb) on the surface of layered Ti_3C_2 materials to prepare a mediator-free biosensor for nitrite detection [93]. Among them, the morphology of the Nafion/Hb/Ti_3C_2 composite film is shown in the Fig. 8G. Compared with the GCE electrode, the Nafion/Hb/-Ti_3C_2/GCE electrode's effective surface area increases significantly. Ti_3C_2 with a high surface area can easily capture substrates and access the enzymes immobilized on nanomaterials. The sensor's performance is improved by the increased likelihood of efficient collisions between substrates and redox proteins. The constructed biosensor is beneficial to the direct electron transfer and has a excellent electrochemical activity to detect $NaNO_2$. For NO^{2-}, this biosensor had a low limit of detection of 0.12 μM and a broad linear range of 0.5 μM–11.8 mM (Fig. 8F). It demonstrates that Ti_3C_2 is a potential nanomaterial for protein immobilization and mediator-free biosensors.

3.3.3. *Heavy metals sensor*

Toxic heavy metals can be harmful to the environment and human health [142–145]. Zhu et al. used acid etching and alkali intercalation treatment to synthesize alk-Ti_3C_2. And it is proven that it is a new platform for the simultaneous electrochemical to detect various heavy metal ions using square wave anodic stripping voltammetry [94]. Compared with Ti_3C_2 modified electrodes [146], alk-Ti_3C_2 modified electrodes have unique morphology and surface chemical properties and have better electrochemical response performance. The key operating parameters are optimized to determine trace heavy metal ions. The method has high sensitivity and good linearity, and the limits of detection for Cd(II), Pb(II), Cu(II), and Hg(II) are 98 nM, 41 nM, 32 nM and 0.13 μM, respectively. This method brings an avenue for using MXenes in the detection of heavy metals.

Lv et al. composited $Ti_3C_2T_x$ with protonated carbon nitride (H–C_3N_4/$Ti_3C_2T_x$) to synthesize a highly sensitive electrochemical sensor to detect heavy metal ions (HMIs) [95]. Due to the electrostatic interaction, a large amount of H–C_3N_4 is distributed on the surface of $Ti_3C_2T_x$ as a coating material. The conductivity of H–C_3N_4/$Ti_3C_2T_x$ composites originates from $Ti_3C_2T_x$, and H–C_3N_4 provides abundant electroactive deposition sites for the deposition of HMIs. Furthermore, the protective effect of the H–C_3N_4 coating improved the stability of the H–C_3N_4/$Ti_3C_2T_x$ composite. The H–C_3N_4/$Ti_3C_2T_x$ electrode has a high sensitivity to simultaneous detect Cd^{2+} (50 nM ~ 1.5 μM) and Pb^{2+} (50 nM ~ 1.5 μM), with detection limits of 1 nM and 0.6 nM, respectively. Especially, the H–C_3N_4/$Ti_3C_2T_x$ composite-based sensor exhibited good selectivity for Cd^{2+} and Pb^{2+} in the presence of interfering ions and molecules. The H–C_3N_4/$Ti_3C_2T_x$ electrode's good reproducibility and stabilitysuggest that the sensor has great application prospects in industrial sewage treatment and other commercial fields.

4. Conclusions

Since the discovery of MXenes in 2011, great progress has been achieved in the synthesis, surface modification, and application of MXenes in a wide range of fields such as energy storage, catalysis,

electronics and environmental remediation. This paper discusses the latest synthesis and surface functionalization strategies for mass production and applications in different fields. In addition, this paper reviews the MXenes nanocomposites' structural properties and their applications as electrochemical (biological) sensors in clinical biomarkers, drugs, pesticides, and other aspects. In this paper, the electrochemical properties and practical applications are systematically discussed sensitivity, dynamic range, and detection limit. It is worth noting that the Mxene-based enzyme sensor is very stable because its unique accordion-like structure allows efficient fixation of the enzyme and Provide a good environment for the enzyme to maintain its biological activity. MXenes have high metal conductivity, composition variability and good hydrophilicity, and are suitable to construct electrochemical sensors. So, as a sensitive electrochemical sensor detecting various analytes, MXenes has broad application prospects. Hope this review will provide a clear vision for the future commercialization of Mxene-based sensors and encourage extensive research.

References

[1] M. Naguib, M. Kurtoglu, V. Presser, J. Lu, J. Niu, M. Heon, L. Hultman, Y. Gogotsi, M.W. Barsoum, Two-dimensional nanocrystals produced by exfoliation of Ti_3AlC_2, Adv. Mater. 23 (37) (2011) 4248–4253.
[2] M.R. Lukatskaya, O. Mashtalir, C.E. Ren, Y. Dall'Agnese, P. Rozier, P.L. Taberna, M. Naguib, P. Simon, M.W. Barsoum, Y. Gogotsi, Cation intercalation and high volumetric capacitance of two-dimensional titanium carbide, Science 341 (6153) (2013) 1502–1505.
[3] M. Alhabeb, K. Maleski, B. Anasori, P. Lelyukh, L. Clark, S. Sin, Y. Gogotsi, Guidelines for synthesis and processing of two-dimensional titanium carbide ($Ti_3C_2T_x$ MXene), Chem. Mater. 29 (18) (2017) 7633–7644.
[4] P. Ares, K. Novoselov, Recent advances in graphene and other 2D materials, Nano Mater. Sci. 4 (2022), https://doi.org/10.1016/j.nanoms.2021.05.002.
[5] G. Liu, Y. Xu, T. Yang, L. Jiang, Recent advances in electrocatalysts for seawater splitting, Nano Mater. Sci. (2020), https://doi.org/10.1016/j.nanoms.2020.12.003.
[6] K. Chen, Y. Xu, Y. Zhao, J. Li, X. Wang, L. Qu, Recent progress in graphene-based wearable piezoresistive sensors: From 1D to 3D device geometries, Nano Mater. Sci. (2022), https://doi.org/10.1016/j.nanoms.2021.11.003.
[7] F. Li, Y. Li, J. Qu, J. Wang, V.K. Bandari, F. Zhu, O.G. Schmidt, Recent developments of stamped planar micro-supercapacitors: materials, fabrication and perspectives, Nano Mater. Sci. 3 (2) (2021) 154–169.
[8] M. Naguib, V.N. Mochalin, M.W. Barsoum, Y. Gogotsi, 25th anniversary article: MXenes: a new family of two-dimensional materials, Adv. Mater. 26 (7) (2014) 992–1005.
[9] R. Chen, N. Han, L. Li, S. Wang, X. Ma, C. Wang, H. Li, H. Li, L. Zeng, Fundamental understanding of oxygen content in activated carbon on acetone adsorption desorption, Appl. Surf. Sci. 508 (2020), 145211.
[10] N. Han, S. Feng, W. Guo, O.M. Mora, X. Zhao, W. Zhang, S. Xie, Z. Zhou, Z. Liu, Q. Liu, K. Wan, X. Zhang, J. Fransaer, Rational design of Ruddlesden–Popper perovskite electrocatalyst for oxygen reduction to hydrogen peroxide, SusMat (2022), https://doi.org/10.1002/sus2.71.
[11] P. Lakhe, E.M. Prehn, T. Habib, J.L. Lutkenhaus, M. Radovic, M.S. Mannan, M.J. Green, Process safety analysis for $Ti_3C_2T_x$ MXene synthesis and processing, Ind. Eng. Chem. Res. 58 (4) (2019) 1570–1579.
[12] C. Jiang, C. Wu, X. Li, Y. Yao, L. Lan, F. Zhao, Z. Ye, Y. Ying, J. Ping, All-electrospun flexible triboelectric nanogenerator based on metallic MXene nanosheets, Nano Energy 59 (2019) 268–276.
[13] Z. Xu, G. Liu, H. Ye, W. Jin, Z. Cui, Two-dimensional MXene incorporated chitosan mixed-matrix membranes for efficient solvent dehydration, J. Membr. Sci. 563 (2018) 625–632.
[14] S. Fu, Z. Sun, P. Huang, Y. Li, N. Hu, Some basic aspects of polymer nanocomposites: a critical review, Nano Mater. Sci. 1 (1) (2019) 2–30.
[15] Y. Sun, W. Zhang, Q. Wang, N. Han, A. Núñez-Delgado, Y. Cao, W. Si, F. Wang, S. Liu, Biomass-derived N, S co-doped 3D multichannel carbon supported Au@Pd@Pt catalysts for oxygen reduction, Environ. Res. 202 (2021).
[16] L. Gao, C. Li, W. Huang, S. Mei, H. Lin, Q. Ou, Y. Zhang, J. Guo, F. Zhang, S. Xu, H. Zhang, MXene/Polymer membranes: synthesis, properties, and emerging applications, Chem. Mater. 32 (5) (2020) 1703–1747.
[17] N. Han, X. Guo, J. Cheng, P. Liu, S. Zhang, S. Huang, M.R. Rowles, J. Fransaer, S. Liu, Inhibiting in situ phase transition in Ruddlesden-Popper perovskite via tailoring bond hybridization and its application in oxygen permeation, Matter 4 (5) (2021) 1720–1734.
[18] N. Han, P. Liu, J. Jiang, L. Ai, Z. Shao, S. Liu, Recent advances in nanostructured metal nitrides for water splitting, J. Mater. Chem. 6 (41) (2018) 19912–19933.
[19] M.E. Genovese, S. Abraham, G. Caputo, G. Nanni, S.K. Kumaran, C.D. Montemagno, A. Athanassiou, D. Fragouli, Photochromic paper indicators for acidic food spoilage detection, ACS Omega 3 (10) (2018) 13484–13493.
[20] X. Fu, L. Wang, L. Zhao, Z. Yuan, Y. Zhang, D. Wang, D. Wang, J. Li, D. Li, V. Shulga, G. Shen, W. Han, Controlled assembly of MXene nanosheets as an electrode and active layer for high-performance electronic skin, Adv. Funct. Mater. 31 (17) (2021), 2010533.
[21] W. Hou, Y. Sun, Y. Zhang, T. Wang, L. Wu, Y. Du, W. Zhong, Mixed-dimensional heterostructure of few-layer MXene based vertical aligned MoS_2 nanosheets for enhanced supercapacitor performance, J. Alloys Compd. 859 (2021), 157797.
[22] K. Rajavel, X. Yu, P. Zhu, Y. Hu, R. Sun, C. Wong, Exfoliation and defect control of two-dimensional few-layer MXene Ti3C2Tx for electromagnetic interference shielding coatings, ACS Appl. Mater. Interfaces 12 (44) (2020) 49737–49747.
[23] B. Yang, L. Wang, M. Zhang, W. Li, Q. Zhou, L. Zhong, Advanced separators based on aramid nanofiber (ANF) membranes for lithium-ion batteries: a review of recent progress, J. Mater. Chem. 9 (22) (2021) 12923–12946.
[24] M. Jose, G. Oudebrouckx, S. Bormans, P. Veske, R. Thoelen, W. Deferme, Monitoring body fluids in textiles: combining impedance and thermal principles in a printed, wearable, and washable sensor, ACS Sens. 6 (3) (2021) 896–907.
[25] W. Niu, X. Cao, Y. Wang, B. Yao, Y. Zhao, J. Cheng, S. Wu, S. Zhang, X. He, Photonic vitrimer elastomer with self-healing, high toughness, mechanochromism, and excellent durability based on dynamic covalent bond, Adv. Funct. Mater. 31 (13) (2021), 2009017.
[26] A. Angelucci, M. Cavicchioli, I.A. Cintorrino, G. Lauricella, C. Rossi, S. Strati, A. Aliverti, Smart textiles and sensorized garments for physiological monitoring: a review of available solutions and techniques, Sensors 21 (3) (2021).
[27] L. Wang, L. Wu, Y. Wang, J. Luo, H. Xue, J. Gao, Drop casting based superhydrophobic and electrically conductive coating for high performance strain sensing, Nano Mater. Sci. 4 (2) (2022).
[28] S. Zheng, H. Wang, P. Das, Y. Zhang, Y. Cao, J. Ma, S. Liu, Z.-S. Wu, Multitasking MXene inks enable high-performance printable microelectrochemical energy storage devices for all-flexible self-powered integrated systems, Adv. Mater. 33 (10) (2021), 2005449.
[29] K. Bayoumy, M. Gaber, A. Elshafeey, O. Mhaimeed, E.H. Dineen, F.A. Marvel, S.S. Martin, E.D. Muse, M.P. Turakhia, K.G. Tarakji, M.B. Elshazly, Smart wearable devices in cardiovascular care: where we are and how to move forward, Nat. Rev. Cardiol. 18 (8) (2021) 581–599.
[30] J. Park, Y. Lee, J. Hong, Y. Lee, M. Ha, Y. Jung, H. Lim, S.Y. Kim, H. Ko, Tactile-direction-sensitive and stretchable electronic skins based on human-skin-inspired interlocked microstructures, ACS Nano 8 (12) (2014) 12020–12029.
[31] P.K. Kalambate, Z. Huang Dhanjai, Y. Li, Y. Shen, M. Xie, Y. Huang, A.K. Srivastava, Core@shell nanomaterials based sensing devices: a review, TrAC, Trends Anal. Chem. 115 (2019) 147–161.
[32] P.K. Kalambate, Y. Li, Y. Shen, Y. Huang, Mesoporous Pd@Pt core–shell nanoparticles supported on multi-walled carbon nanotubes as a sensing platform: application in simultaneous electrochemical detection of anticancer drugs doxorubicin and dasatinib, Anal. Methods 11 (4) (2019) 443–453.
[33] N. Han, M. Race, W. Zhang, R. Marotta, C. Zhang, A. Bokhari, J.J. Klemeš, Perovskite and related oxide based electrodes for water splitting, J. Clean. Prod. 318 (2021), 128544.
[34] N. Han, Z. Shen, X. Zhao, R. Chen, V.K. Thakur, Perovskite oxides for oxygen transport: chemistry and material horizons, Sci. Total Environ. 806 (2022), 151213.
[35] P.K. Kalambate, M.R. Biradar, S.P. Karna, A.K. Srivastava, Adsorptive stripping differential pulse voltammetry determination of rivastigmine at graphene nanosheet-gold nanoparticle/carbon paste electrode, J. Electroanal. Chem. 757 (2015) 150–158.
[36] P.K. Kalambate, C.R. Rawool, A.K. Srivastava, Voltammetric determination of pyrazinamide at graphene-zinc oxide nanocomposite modified carbon paste electrode employing differential pulse voltammetry, Sensors Actuat. B Chem. 237 (2016) 196–205.
[37] M. Chen, Z. Li, L. Chen, Highly antibacterial rGO/Cu_2O nanocomposite from a biomass precursor: synthesis, performance, and mechanism, Nano Mater. Sci. 2 (2) (2020) 172–179.
[38] A. Sinha, B. Tan Dhanjai, Y. Huang, H. Zhao, X. Dang, J. Chen, R. Jain, MoS2 nanostructures for electrochemical sensing of multidisciplinary targets: a review, TrAC, Trends Anal. Chem. 102 (2018) 75–90.
[39] Z.-H. Tang, W.-B. Zhu, J.-Z. Chen, Y.-Q. Li, P. Huang, K. Liao, S.-Y. Fu, Flexible and electrically robust graphene-based nanocomposite paper with hierarchical microstructures for multifunctional wearable devices, Nano Mater. Sci (2021).
[40] H. Wang, Y. Wu, X. Yuan, G. Zeng, J. Zhou, X. Wang, J.W. Chew, Clay-inspired MXene-based electrochemical devices and photo-electrocatalyst: state-of-the-art progresses and challenges, Adv. Mater. 30 (12) (2018), e1704561.
[41] M.W. Barsoum, The $M_{N+1}AX_N$ phases: a new class of solids: thermodynamically stable nanolaminates, Prog. Solid State Chem. 28 (1–4) (2000) 201–281.
[42] Z. Sun, D. Music, R. Ahuja, S. Li, J.M. Schneider, Bonding and classification of nanolayered ternary carbides, Phys. Rev. B 70 (9) (2004).
[43] Q. Wang, N. Han, A. Bokhari, X. Li, Y. Cao, S. Asif, Z. Shen, W. Si, F. Wang, J.J. Klemeš, X. Zhao, Insights into MXenes-based electrocatalysts for oxygen reduction, Energy (2022), 124465.
[44] K.S. Novoselov, A.K. Geim, S.V. Morozov, D. Jiang, M.I. Katsnelson, I.V. Grigorieva, S.V. Dubonos, A.A. Firsov, Two-dimensional gas of massless Dirac fermions in graphene, Nature 438(7065) (2005) 197–200.
[45] M. Naguib, O. Mashtalir, J. Carle, V. Presser, J. Lu, L. Hultman, Y. Gogotsi, M.W. Barsoum, Two-dimensional transition metal carbides, ACS Nano 6 (2) (2012) 1322–1331.
[46] O. Mashtalir, M.R. Lukatskaya, M.Q. Zhao, M.W. Barsoum, Y. Gogotsi, Amine-assisted delamination of Nb_2C MXene for Li-ion energy storage devices, Adv. Mater. 27 (23) (2015) 3501–3506.
[47] M. Alhabeb, K. Maleski, T.S. Mathis, A. Sarycheva, C.B. Hatter, S. Uzun, A. Levitt, Y. Gogotsi, Selective etching of silicon from Ti_3SiC_2 (MAX) to obtain 2D titanium carbide (MXene), Chem. Int. Ed. Engl 57 (19) (2018) 5444–5448.
[48] J. Halim, S. Kota, M.R. Lukatskaya, M. Naguib, M.-Q. Zhao, E.J. Moon, J. Pitock, J. Nanda, S.J. May, Y. Gogotsi, M.W. Barsoum, Synthesis and characterization of 2D molybdenum carbide (MXene), Adv. Funct. Mater. 26 (18) (2016) 3118–3127.

[49] J. Zhou, X. Zha, F.Y. Chen, Q. Ye, P. Eklund, S. Du, Q. Huang, A two-dimensional zirconium carbide by selective etching of Al_3C_3 from nanolaminated $Zr_3Al_3C_5$, Chem. Int. Ed. Engl 55 (16) (2016) 5008–5013.
[50] J. Halim, M.R. Lukatskaya, K.M. Cook, J. Lu, C.R. Smith, L.A. Naslund, S.J. May, L. Hultman, Y. Gogotsi, P. Eklund, M.W. Barsoum, Transparent conductive two-dimensional titanium carbide epitaxial thin films, Chem. Mater. 26 (7) (2014) 2374–2381.
[51] M. Ghidiu, M.R. Lukatskaya, M.Q. Zhao, Y. Gogotsi, M.W. Barsoum, Conductive two-dimensional titanium carbide 'clay' with high volumetric capacitance, Nature 516 (7529) (2014) 78–81.
[52] A. Feng, Y. Yu, Y. Wang, F. Jiang, Y. Yu, L. Mi, L. Song, Two-dimensional MXene Ti_3C_2 produced by exfoliation of Ti_3AlC_2, Mater. Des. 114 (2017) 161–166.
[53] X. Wang, C. Garnero, G. Rochard, D. Magne, S. Morisset, S. Hurand, P. Chartier, J. Rousseau, T. Cabioc'h, C. Coutanceau, V. Mauchamp, S. Célérier, A new etching environment (FeF_3/HCl) for the synthesis of two-dimensional titanium carbide MXenes: a route towards selective reactivity vs, water, J. Mater. Chem. A 5 (41) (2017) 22012–22023.
[54] M. Malaki, A. Maleki, R.S. Varma, MXenes and ultrasonication, J. Mater. Chem. 7 (18) (2019) 10843–10857.
[55] V. Natu, R. Pai, M. Sokol, M. Carey, V. Kalra, M.W. Barsoum, 2D $Ti_3C_2T_z$ MXene synthesized by water-free etching of Ti_3AlC_2 in polar organic solvents, Chem 6 (3) (2020) 616–630.
[56] N. Han, S. Wang, Z. Yao, W. Zhang, X. Zhang, L. Zeng, R. Chen, Superior three-dimensional perovskite catalyst for catalytic oxidation, EcoMat 2 (3) (2020), e12044.
[57] N. Han, Z. Yao, H. Ye, C. Zhang, P. Liang, H. Sun, S. Wang, S. Liu, Efficient removal of organic pollutants by ceramic hollow fibre supported composite catalyst, Sustain. Mater. Techno 20 (2019), e00108.
[58] S. Wang, W. Zhang, F. Jia, H. Fu, T. Liu, X. Zhang, B. Liu, A. Núñez-Delgado, N. Han, Novel Ag_3PO_4/boron-carbon-nitrogen photocatalyst for highly efficient degradation of organic pollutants under visible-light irradiation, J. Environ. Manag. 292 (2021), 112763.
[59] P. Urbankowski, B. Anasori, T. Makaryan, D. Er, S. Kota, P.L. Walsh, M. Zhao, V.B. Shenoy, M.W. Barsoum, Y. Gogotsi, Synthesis of two-dimensional titanium nitride Ti_4N_3 (MXene), Nanoscale 8 (22) (2016) 11385–11391.
[60] H. Kumar, N.C. Frey, L. Dong, B. Anasori, Y. Gogotsi, V.B. Shenoy, Tunable magnetism and transport properties in nitride MXenes, ACS Nano 11 (8) (2017) 7648–7655.
[61] N. Han, W. Zhang, W. Guo, S. Xie, C. Zhang, X. Zhang, J. Fransaer, S. Liu, Novel oxygen permeable hollow fiber perovskite membrane with surface wrinkles, Separ. Purif. Technol. 261 (2021), 118295.
[62] Y. Orooji, N. Han, Z. Nezafat, N. Shafiei, Z. Shen, M. Nasrollahzadeh, H. Karimi-Maleh, R. Luque, A. Bokhari, J.J. Klemeš, Valorisation of nuts biowaste: prospects in sustainable bio(nano)catalysts and environmental applications, J. Clean. Prod. 347 (2022), 131220.
[63] M. Li, J. Lu, K. Luo, Y. Li, K. Chang, K. Chen, J. Zhou, J. Rosen, L. Hultman, P. Eklund, P.O.A. Persson, S. Du, Z. Chai, Z. Huang, Q. Huang, Element replacement approach by reaction with Lewis acidic molten salts to synthesize nanolaminated MAX phases and MXenes, J. Am. Chem. Soc. 141 (11) (2019) 4730–4737.
[64] J. Sun, L. Wang, S. Zhang, Z. Li, X. Zhang, W. Dai, R. Mori, ZnCl2/phosphonium halide: an efficient Lewis acid/base catalyst for the synthesis of cyclic carbonate, J. Mol. Catal. Chem. 256 (1–2) (2006) 295–300.
[65] M. Jiang, M. Zhang, L. Wang, Y. Fei, S. Wang, A. Núñez-Delgado, A. Bokhari, M. Race, A. Khataee, J. Jaromír Klemeš, L. Xing, N. Han, Photocatalytic degradation of xanthate in flotation plant tailings by TiO_2/graphene nanocomposites, Chem. Eng. J. 431 (2022), 134104.
[66] N. Han, X. Zhao, V.K. Thakur, Adjusting the interfacial adhesion via surface modification to prepare high-performance fibers, Nano Mater. Sci. (2021), https://doi.org/10.1016/j.nanoms.2021.11.004.
[67] M. Zhang, N. Han, Y. Fei, J. Liu, L. Xing, A. Núñez-Delgado, M. Jiang, S. Liu, TiO_2/g-C_3N_4 photocatalyst for the purification of potassium butyl xanthate in mineral processing wastewater, J. Environ. Manag. 297 (2021), 113311.
[68] Y. Li, H. Shao, Z. Lin, J. Lu, L. Liu, B. Duployer, P.O.A. Persson, P. Eklund, L. Hultman, M. Li, K. Chen, X.H. Zha, S. Du, P. Rozier, Z. Chai, E. Raymundo-Pinero, P.L. Taberna, P. Simon, Q. Huang, A general Lewis acidic etching route for preparing MXenes with enhanced electrochemical performance in non-aqueous electrolyte, Nat. Mater. 19 (8) (2020) 894–899.
[69] V. Kamysbayev, A.S. Filatov, H. Hu, X. Rui, F. Lagunas, D. Wang, R.F. Klie, D.V. Talapin, Covalent surface modifications and superconductivity of two-dimensional metal carbide MXenes, Science 369 (6506) (2020) 979–983.
[70] S. Yang, P. Zhang, F. Wang, A.G. Ricciardulli, M.R. Lohe, P.W.M. Blom, X. Feng, Fluoride-free synthesis of two-dimensional titanium carbide (MXene) using A binary aqueous system, Chem. Int. Ed. Engl 57 (47) (2018) 15491–15495.
[71] T. Li, L. Yao, Q. Liu, J. Gu, R. Luo, J. Li, X. Yan, W. Wang, P. Liu, B. Chen, W. Zhang, W. Abbas, R. Naz, D. Zhang, Fluorine-free synthesis of high-purity $Ti_3C_2T_x$ (T=OH, O) via alkali treatment, Chem. Int. Ed. Engl 57 (21) (2018) 6115–6119.
[72] C. Xu, L. Wang, Z. Liu, L. Chen, J. Guo, N. Kang, X.L. Ma, H.M. Cheng, W. Ren, Large-area high-quality 2D ultrathin Mo_2C superconducting crystals, Nat. Mater. 14 (11) (2015) 1135–1141.
[73] A. VahidMohammadi, J. Rosen, Y. Gogotsi, The world of two-dimensional carbides and nitrides (MXenes), Science 372 (6547) (2021).
[74] X. Li, M. Li, Q. Yang, G. Liang, Z. Huang, L. Ma, D. Wang, F. Mo, B. Dong, Q. Huang, C. Zhi, In situ electrochemical synthesis of MXenes without acid/alkali usage in/for an aqueous zinc ion battery, Adv. Energy Mater. 10 (36) (2020).
[75] R. Ramachandran, C. Zhao, M. Rajkumar, K. Rajavel, P. Zhu, W. Xuan, Z.-X. Xu, F. Wang, Porous nickel oxide microsphere and $Ti_3C_2T_x$ hybrid derived from metal-organic framework for battery-type supercapacitor electrode and non-enzymatic H_2O_2 sensor, Electrochim. Acta 322 (2019).
[76] F. Wang, C. Yang, C. Duan, D. Xiao, Y. Tang, J. Zhu, An organ-like titanium carbide material (MXene) with multilayer structure encapsulating hemoglobin for a mediator-free biosensor, J. Electrochem. Soc. 162 (1) (2014) B16–B21.
[77] F. Wang, C. Yang, M. Duan, Y. Tang, J. Zhu, TiO_2 nanoparticle modified organ-like Ti_3C_2 MXene nanocomposite encapsulating hemoglobin for a mediator-free biosensor with excellent performances, Biosens. Bioelectron. 74 (2015) 1022–1028.
[78] L. Lorencova, T. Bertok, E. Dosekova, A. Holazova, D. Paprckova, A. Vikartovska, V. Sasinkova, J. Filip, P. Kasak, M. Jerigova, D. Velic, K.A. Mahmoud, J. Tkac, Electrochemical performance of $Ti_3C_2T_x$ MXene in aqueous media: towards ultrasensitive H_2O_2 sensing, Electrochim. Acta 235 (2017) 471–479.
[79] L. Lorencova, T. Bertok, J. Filip, M. Jerigova, D. Velic, P. Kasak, K.A. Mahmoud, J. Tkac, Highly stable $Ti_3C_2T_x$ (MXene)/Pt nanoparticles-modified glassy carbon electrode for H_2O_2 and small molecules sensing applications, Sensors Actuat. B Chem. 263 (2018) 360–368.
[80] R. Gao, X. Yang, Q. Yang, Y. Wu, F. Wang, Q. Xia, S.J. Bao, Design of an amperometric glucose oxidase biosensor with added protective and adhesion layers, Mikrochim. Acta 188 (9) (2021) 312.
[81] M. Li, L. Fang, H. Zhou, F. Wu, Y. Lu, H. Luo, Y. Zhang, B. Hu, Three-dimensional porous MXene/NiCo-LDH composite for high performance non-enzymatic glucose sensor, Appl. Surf. Sci. 495 (2019).
[82] H.L. Chia, C.C. Mayorga-Martinez, N. Antonatos, Z. Sofer, J.J. Gonzalez-Julian, R.D. Webster, M. Pumera, MXene titanium carbide-based biosensor: strong dependence of exfoliation method on performance, Anal. Chem. 92 (3) (2020) 2452–2459.
[83] T. Xia, G. Liu, J. Wang, S. Hou, S. Hou, MXene-based enzymatic sensor for highly sensitive and selective detection of cholesterol, Biosens. Bioelectron. 183 (2021), 113243.
[84] X. Liu, L. He, P. Li, X. Li, P. Zhang, A direct electrochemical H_2S sensor based on $Ti_3C_2T_x$ MXene, Chemelectrochem 8 (19) (2021) 3658–3665.
[85] H. Wang, H. Li, Y. Huang, M. Xiong, F. Wang, C. Li, A label-free electrochemical biosensor for highly sensitive detection of gliotoxin based on DNA nanostructure/MXene nanocomplexes, Biosens. Bioelectron. 142 (2019), 111531.
[86] F. Shahzad, A. Iqbal, S.A. Zaidi, S.-W. Hwang, C.M. Koo, Nafion-stabilized two-dimensional transition metal carbide ($Ti_3C_2T_x$ MXene) as a high-performance electrochemical sensor for neurotransmitter, J. Ind. Eng. Chem. 79 (2019) 338–344.
[87] M. Zhang, Y. Yang, Y. Wang, B. Zhang, H. Wang, G. Fang, S. Wang, A molecularly imprinted electrochemical sensor based on cationic intercalated two-dimensional titanium carbide nanosheets for sensitive and selective detection of triclosan in food samples, Food Control 132 (2022).
[88] W. Zhong, F. Gao, J. Zou, S. Liu, M. Li, Y. Gao, Y. Yu, X. Wang, L. Lu, MXene@Ag-based ratiometric electrochemical sensing strategy for effective detection of carbendazim in vegetable samples, Food Chem. 360 (2021), 130006.
[89] Y. Xie, F. Gao, X. Tu, X. Ma, Q. Xu, R. Dai, X. Huang, Y. Yu, L. Lu, Facile synthesis of MXene/electrochemically reduced graphene oxide composites and their application for electrochemical sensing of carbendazim, J. Electrochem. Soc. 166 (16) (2019) B1673–B1680.
[90] Y. Jiang, X. Zhang, L. Pei, S. Yue, L. Ma, L. Zhou, Z. Huang, Y. He, J. Gao, Silver nanoparticles modified two-dimensional transition metal carbides as nanocarriers to fabricate acetycholinesterase-based electrochemical biosensor, Chem. Eng. J. 339 (2018) 547–556.
[91] Q. Xu, S. Chen, J. Xu, X. Duan, L. Lu, Q. Tian, X. Zhang, Y. Cai, X. Lu, L. Rao, Y. Yu, Facile synthesis of hierarchical MXene/ZIF-67/CNTs composite for electrochemical sensing of luteolin, J. Electroanal. Chem. 880 (2021).
[92] Y. Yao, X. Han, X. Yang, J. Zhao, C. Chai, Detection of hydrazine at MXene/ZIF-8 nanocomposite modified electrode†, Chin. J. Chem. 39 (2) (2021) 330–336.
[93] H. Liu, C. Duan, C. Yang, W. Shen, F. Wang, Z. Zhu, A novel nitrite biosensor based on the direct electrochemistry of hemoglobin immobilized on MXene-Ti_3C_2, Sensors Actuat. B Chem. 218 (2015) 60–66.
[94] X. Zhu, B. Liu, H. Hou, Z. Huang, K.M. Zeinu, L. Huang, X. Yuan, D. Guo, J. Hu, J. Yang, Alkaline intercalation of Ti_3C_2 MXene for simultaneous electrochemical detection of Cd(II), Pb(II), Cu(II) and Hg(II), Electrochim. Acta 248 (2017) 46–57.
[95] X. Lv, F. Pei, S. Feng, Y. Wu, S.-M. Chen, Q. Hao, W. Lei, Facile synthesis of protonated carbon nitride/$Ti_3C_2T_x$ nanocomposite for simultaneous detection of Pb2+ and Cd2+, J. Electrochem. Soc. 167 (6) (2020).
[96] C.L. Sawyers, The cancer biomarker problem, Nature 452 (7187) (2008) 548–552.
[97] S.K. Chatterjee, B.R. Zetter, Cancer biomarkers: knowing the present and predicting the future, Future Oncol. 1 (1) (2005) 37–50.
[98] S. Kumar, A. Mohan, R. Guleria, Biomarkers in cancer screening, research and detection: present and future: a review, Biomarkers 11 (5) (2006) 385–405.
[99] P.R. Srinivas, B.S. Kramer, S. Srivastava, Trends in biomarker research for cancer detection, Lancet Oncol. 2 (11) (2001) 698–704.
[100] M. Verma, S. Srivastava, New cancer biomarkers deriving from NCI early detection research, in: H.-J. Senn, R. Morant (Eds.), Tumor Prevention and Genetics, Springer Berlin Heidelberg, Berlin, Heidelberg, 2003, pp. 72–84.
[101] J.F. Rusling, C.V. Kumar, J.S. Gutkind, V. Patel, Measurement of biomarker proteins for point-of-care early detection and monitoring of cancer, Analyst 135 (10) (2010) 2496–2511.
[102] Y. Wang, N. Han, X. Li, S. Yu, L. Xing, Artificial light-harvesting systems and their applications in photocatalysis and cell labeling, ChemPhysMater (2022), https://doi.org/10.1016/j.chphma.2022.05.002.

[103] M. Carpelan-Holmström, J. Louhimo, U.H. Stenman, H. Alfthan, C. Haglund, CEA, CA 19-9 and CA 72-4 improve the diagnostic accuracy in gastrointestinal cancers, Anticancer Res. 22 (4) (2002) 2311–2316.
[104] T. Hayakawa, S. Naruse, M. Kitagawa, H. Ishiguro, T. Kondo, K. Kurimoto, M. Fukushima, T. Takayama, Y. Horiguchi, N. Kuno, A. Noda, T. Furukawa, A prospective multicenter trial evaluating diagnostic validity of multivariate analysis and individual serum marker in differential diagnosis of pancreatic cancer from benign pancreatic diseases, Int. J. Pancreatol. 25 (1) (1999) 23–29.
[105] W. Zhang, N. Han, J. Luo, X. Han, S. Feng, W. Guo, S. Xie, Z. Zhou, P. Subramanian, K. Wan, J. Arbiol, C. Zhang, S. Liu, M. Xu, X. Zhang, J. Fransaer, Critical role of phosphorus in hollow structures cobalt-based phosphides as bifunctional catalysts for water splitting, Small 18 (4) (2022), 2103561.
[106] M. Sawangphruk, Y. Sanguansak, A. Krittayavathananon, S. Luanwuthi, P. Srimuk, S. Nilmoung, S. Maensiri, W. Meevasana, J. Limtrakul, Silver nanodendrite modified graphene rotating disk electrode for nonenzymatic hydrogen peroxide detection, Carbon 70 (2014) 287–294.
[107] Y. Cao, W. Si, Q. Hao, Z. Li, W. Lei, X. Xia, J. Li, F. Wang, Y. Liu, One-pot fabrication of Hemin-N C composite with enhanced electrocatalysis and application to H_2O_2 sensing, Electrochim. Acta 261 (2018) 206–213.
[108] Y. Cao, Y. Qi, X. Meng, W. Si, Q. Hao, W. Lei, J. Li, J. Cao, X. Li, Q. Li, F. Wang, Facile preparation of hemin/polypyrrole/N, B-Co-doped graphene nanocomposites for non-enzymatic H_2O_2 determination, J. Electrochem. Soc. 165 (13) (2018) B623–B631.
[109] Y. Jiang, X. Zhao, Q. Wang, Y. Sun, Y. Cao, N. Han, C. Lee, J. Cao, J. Li, W. Si, Facile synthesis of paper-derived porous activated carbon and the electrochemical determination of hydrogen peroxide, J. Electrochem. Soc. 169 (5) (2022).
[110] M.H. Hussain, L.P. Fook, M.K. Sanira Putri, H.L. Tan, N.F. Abu Bakar, N. Radacsi, Advances on ultra-sensitive electrospun nanostructured electrochemical and colorimetric sensors for diabetes mellitus detection, Nano Mater. Sci. 3 (4) (2021) 321–343.
[111] Y. Li, J. Qu, F. Li, Z. Qu, H. Tang, L. Liu, M. Zhu, O.G. Schmidt, Advanced architecture designs towards high-performance 3D microbatteries, Nano Mater. Sci. 3 (2) (2021) 140–153.
[112] Y. Wan, Y. Liu, D. Chao, W. Li, D. Zhao, Recent advances in hard carbon anodes with high initial Coulombic efficiency for sodium-ion batteries, Nano Mater. Sci (2022).
[113] Y. Cheng, Y. Ma, L. Li, M. Zhu, Y. Yue, W. Liu, L. Wang, S. Jia, C. Li, T. Qi, J. Wang, Y. Gao, Bioinspired microspines for a high-performance spray Ti3C2Tx MXene-based piezoresistive sensor, ACS Nano 14(2) (2020) 2145–2155.
[114] A. Devadoss, J.D. Burgess, Steady-state detection of cholesterol contained in the plasma membrane of a single cell using lipid bilayer-modified microelectrodes incorporating cholesterol oxidase, J. Am. Chem. Soc. 126 (33) (2004) 10214–10215.
[115] Y. Cao, W. Si, Y. Zhang, Q. Hao, W. Lei, X. Xia, J. Li, F. Wang, Nitrogen-doped graphene: effect of graphitic-N on the electrochemical sensing properties towards acetaminophen, FlatChem 9 (2018) 1–7.
[116] Y. Cao, W. Zhang, Y. Sun, Y. Jiang, N. Han, J. Zou, W. Si, F. Wang, A. Nunez-Delgado, S. Liu, Highly active iron-nitrogen-boron-carbon bifunctional electrocatalytic platform for hydrogen peroxide sensing and oxygen reduction, Environ. Res. 201 (2021), 111563.
[117] S. Huang, E. Yang, J. Yao, X. Chu, Y. Liu, Y. Zhang, Q. Xiao, Nitrogen, cobalt Co-doped fluorescent magnetic carbon dots as ratiometric fluorescent probes for cholesterol and uric acid in human blood serum, ACS Omega 4 (5) (2019) 9333–9342.
[118] M. Amiri, S. Arshi, An overview on electrochemical determination of cholesterol, Electroanalysis 32 (7) (2020) 1391–1407.
[119] P. Nagy, Z. Pálinkás, A. Nagy, B. Budai, I. Tóth, A. Vasas, Chemical aspects of hydrogen sulfide measurements in physiological samples, Biochimica et Biophysica Acta BBA, Gen. Subjects 1840 (2) (2014) 876–891.
[120] H. Xu, H. Shang, Q. Liu, C. Wang, J. Di, C. Chen, L. Jin, Y. Du, Dual mode electrochemical-photoelectrochemical sensing platform for hydrogen sulfide detection based on the inhibition effect of titanium dioxide/bismuth tungstate/silver heterojunction, J. Colloid Interface Sci. 581 (2021) 323–333.
[121] M. Asif, A. Aziz, Z. Wang, G. Ashraf, J. Wang, H. Luo, X. Chen, F. Xiao, H. Liu, Hierarchical CNTs@CuMn layered double hydroxide nanohybrid with enhanced electrochemical performance in H_2S detection from live cells, Anal. Chem. 91 (6) (2019) 3912–3920.
[122] X. Ning, D. Tang, M. Zhang, Directly electrospinning submillimeter continuous fibers on tubes to fabricate H_2S detectors with fast and high response, Nano Mater. Sci (2021), https://doi.org/10.1016/j.nanoms.2021.07.005.
[123] D. Brown Gordon, W. Denning David, A.R. Gow Neil, M. Levitz Stuart, G. Netea Mihai, C. White Theodore, Hidden killers: human fungal infections, Sci. Transl. Med. 4 (165) (2012), 165rv13–165rv13.
[124] Z.-H. Sheng, X.-Q. Zheng, J.-Y. Xu, W.-J. Bao, F.-B. Wang, X.-H. Xia, Electrochemical sensor based on nitrogen doped graphene: simultaneous determination of ascorbic acid, dopamine and uric acid, Biosens. Bioelectron. 34 (1) (2012) 125–131.
[125] S.A. Zaidi, Development of molecular imprinted polymers based strategies for the determination of Dopamine, Sensors Actuat, Biol. Chem. 265 (2018) 488–497.
[126] S.A. Zaidi, J.H. Shin, A novel and highly sensitive electrochemical monitoring platform for 4-nitrophenol on MnO2 nanoparticles modified graphene surface, RSC Adv. 5 (108) (2015) 88996–89002.
[127] W. Zhang, J. Zheng, J. Shi, Z. Lin, Q. Huang, H. Zhang, C. Wei, J. Chen, S. Hu, A. Hao, Nafion covered core–shell structured Fe3O4@graphene nanospheres modified electrode for highly selective detection of dopamine, Anal. Chim. Acta 853 (2015) 285–290.
[128] C.-L. Huang, H.-W. Ma, C.-P. Yu, Substance flow analysis and assessment of environmental exposure potential for triclosan in mainland China, Sci, Total Environ 499 (2014) 265–275.
[129] H. Singer, S. Müller, C. Tixier, L. Pillonel, Triclosan: occurrence and fate of a widely used biocide in the aquatic Environment: field measurements in wastewater treatment plants, surface waters, and lake sediments, Environ. Sci. Technol. 36 (23) (2002) 4998–5004.
[130] M. Goodman, D.Q. Naiman, J.S. LaKind, Systematic review of the literature on triclosan and health outcomes in humans, Crit. Rev. Toxicol. 48 (1) (2018) 1–51.
[131] K. Wang, D.-W. Sun, H. Pu, Q. Wei, A rapid dual-channel readout approach for sensing carbendazim with 4-aminobenzenethiol-functionalized core–shell Au@Ag nanoparticles, Analyst 145 (5) (2020) 1801–1809.
[132] S. Singh, N. Singh, V. Kumar, S. Datta, A.B. Wani, D. Singh, K. Singh, J. Singh, Toxicity, monitoring and biodegradation of the fungicide carbendazim, Environ. Chem. Lett. 14 (3) (2016) 317–329.
[133] F. Arduini, F. Ricci, C.S. Tuta, D. Moscone, A. Amine, G. Palleschi, Detection of carbamic and organophosphorous pesticides in water samples using a cholinesterase biosensor based on Prussian Blue-modified screen-printed electrode, Anal. Chim. Acta 580 (2) (2006) 155–162.
[134] F. Gao, X. Chen, H. Tanaka, A. Nishitani, Q. Wang, Alkaline phosphatase mediated synthesis of carbon nanotube–hydroxyapatite nanocomposite and its application for electrochemical determination of luteolin, Adv. Powder Technol. 27 (3) (2016) 921–928.
[135] B. Xu, B. Zhang, L. Yang, F. Zhao, B. Zeng, Electrochemical determination of luteolin using molecularly imprinted poly-carbazole on MoS_2/graphene-carbon nanotubes nanocomposite modified electrode, Electrochim. Acta 258 (2017) 1413–1420.
[136] Y. Ma, Y. Kong, J. Xu, Y. Deng, M. Lu, R. Yu, M. Yuan, T. Li, J. Wang, Carboxyl hydrogel particle film as a local pH buffer for voltammetric determination of luteolin and baicalein, Talanta 208 (2020), 120373.
[137] X. Feng, X. Yin, X. Bo, L. Guo, An ultrasensitive luteolin sensor based on MOFs derived CuCo coated nitrogen-doped porous carbon polyhedron, Sensors Actuat, Biol. Chem. 281 (2019) 730–738.
[138] J. Tang, R. Huang, S. Zheng, S. Jiang, H. Yu, Z. Li, J. Wang, A sensitive and selective electrochemical sensor based on graphene quantum dots/gold nanoparticles nanocomposite modified electrode for the determination of luteolin in peanut hulls, Microchem. J. 145 (2019) 899–907.
[139] M.M. Shahid, P. Rameshkumar, W.J. Basirunc, U. Wijayantha, W.S. Chiu, P.S. Khiew, N.M. Huang, An electrochemical sensing platform of cobalt oxide@gold nanocubes interleaved reduced graphene oxide for the selective determination of hydrazine, Electrochim. Acta 259 (2018) 606–616.
[140] L. Cui, C. Ji, Z. Peng, L. Zhong, C. Zhou, L. Yan, S. Qu, S. Zhang, C. Huang, X. Qian, Y. Xu, Unique tri-output optical probe for specific and ultrasensitive detection of hydrazine, Anal. Chem. 86 (9) (2014) 4611–4617.
[141] L. Cui, Z. Peng, C. Ji, J. Huang, D. Huang, J. Ma, S. Zhang, X. Qian, Y. Xu, Hydrazine detection in the gas state and aqueous solution based on the Gabriel mechanism and its imaging in living cells, Chem. Commun. 50 (12) (2014) 1485–1487.
[142] V. Karri, M. Schuhmacher, V. Kumar, Heavy metals (Pb, Cd, as and MeHg) as risk factors for cognitive dysfunction: a general review of metal mixture mechanism in brain, Environ, Toxicol. Phar 48 (2016) 203–213.
[143] B. Ates, S. Koytepe, A. Ulu, C. Gurses, V.K. Thakur, Chemistry, structures, and advanced applications of nanocomposites from biorenewable resources, Chem. Rev. 120 (2020) 9304–9362.
[144] S.S. Siwal, K. Sheoran, K. Mishra, H. Kaur, A.K. Saini, V. Saini, D.-V.N. Vo, H.Y. Nezhad, V.K. Thakur, Novel synthesis methods and applications of MXene-based nanomaterials (MBNs) for hazardous pollutants degradation: future perspectives, Chemosphere 293 (2022), 133542.
[145] V. Soni, P. Singh, H.H. Phan Quang, A.A. Parwaz Khan, A. Bajpai, Q. Van Le, V.K. Thakur, S. Thakur, V.-H. Nguyen, P. Raizada, Emerging architecture titanium carbide (Ti3C2Tx) MXene based photocatalyst toward degradation of hazardous pollutants: recent progress and perspectives, Chemosphere 293 (2022), 133541.
[146] S. Fu, Z. Sun, P. Huang, H. Li, N. Hu, Some basic aspects of polymer nanocomposites: A critical review, Nano Mater. Sci. 1 (2019) 2–30.